

# NLO QCD corrections to Single Top and W associated photoproduction at the LHC with forward detector acceptances

Hao Sun<sup>1\*</sup>, Wei Liu<sup>1†</sup>, Xiao-Juan Wang<sup>1‡</sup>, Ya-Jin Zhou<sup>2§</sup>, Hong-Sheng Hou<sup>3¶</sup>

<sup>1</sup> Institute of Theoretical Physics, School of Physics & Optoelectronic Technology,  
Dalian University of Technology, Dalian 116024, P.R.China

<sup>2</sup> School of Physics, Shandong University, Jinan, Shandong 250100, P.R.China

<sup>3</sup> Department of Physics, Hangzhou Normal University, Hangzhou 310036, P.R.China

## Abstract

In this paper we study the Single Top and W boson associated photoproduction via the main reaction  $pp \rightarrow p\gamma p \rightarrow pW^{\pm}t + Y$  at the 14 TeV Large Hadron Collider (LHC) up to next-to-leading order (NLO) QCD level assuming a typical LHC multipurpose forward detector. We use the Five-Flavor-Number Schemes (5FNS) with massless bottom quark assumption in the whole calculation. Our results show that the QCD NLO corrections can reduce the scale uncertainty. The typical K-factors are in the range of 1.15 to 1.2 which lead to the QCD NLO corrections of 15% to 20% correspond to the leading-order (LO) predictions with our chosen parameters.

**Keywords:** Single Top, W boson, Forward Detector, Large Hadron Collider

**PACS numbers:** 14.80.Cp, 13.85.Qk

---

\*haosun@mail.ustc.edu.cn    haosun@dlut.edu.cn

†liusd12@mail.dlut.edu.cn

‡wangxiaojuan@mail.dlut.edu.cn

§zhouyj@sdu.edu.cn

¶hshou@hznu.edu.cn

# 1 Introduction

The Large Hadron Collider (LHC) at CERN generates high energetic proton-proton (pp) collisions with a luminosity of  $\mathcal{L} = 10^{34} \text{cm}^{-2} \text{s}^{-1}$  and provides the opportunity to study very high energy physics. After the discovery of Higgs boson[1, 2], probing new physics beyond the Standard Model (BSM) turns to the main goal of the LHC. In such context, studying the heaviest elementary particle, the top quark, is particularly interesting since it is the only fermion with a natural Yukawa coupling to the Higgs boson of the order of unity. Its charged weak coupling might be sensitive to the existence of an additional heavy fermion. These couplings can be probed by measuring specific top quark production cross sections and branching ratios. However, these measurements will be challenging due to the composite internal structure of the colliding particles, i.e., the large QCD or electroweak (EW) backgrounds, the unknown precise centre-of-mass (c.m.s.) energy of the collisions occurring between the partons of protons, the complicate composition of underlying events within the central detector, etc. In this case, very high energy interactions involving quasi-real incoming photons may provide a solution to some of these problems.

General diagrams for the photon induced interactions at the LHC is presented in Fig.1.  $pp \rightarrow p\gamma\gamma p \rightarrow pXp$  [left figure] refers to the photon-photon ( $\gamma\gamma$ ) interaction where photons radiated off by both protons collide and produce a central system X. The system X will be detected by the central detector under clean experimental conditions and the two protons remain intact (namely forward protons), escape from the central detection and continue their path close to the beam line.  $pp \rightarrow p\gamma p \rightarrow pXY$  [right figure] corresponds to photoproduction or photon-proton ( $\gamma p$ ) production: a photon from a proton induces a deep inelastic scattering with the incoming proton and produces a proton remnant Y in addition to the centrally produced X system. Despite a lower available luminosity, photoproduction can occur under better known initial conditions, with fewer final states particles and at high energy scale ( $\sim \text{TeV}$ ), thus can be studied as a complementary tool to normal pp collisions at the LHC. Indeed, the CDF collaboration has already observed such kinds of phenomenon including the exclusive dilepton[3, 4], diphoton[5], dijet [6]

production and charmonium ( $J/\psi$ ) meson photoproduction[7], etc. Both the ATLAS and the CMS collaborations have programs of forward physics. They are devoted to studies of high rapidity regions with extra updated detectors located in a place nearly 100-400m close to the interaction point[8, 9, 10]. Technical details of the ATLAS Forward Physics (AFP) projects can be found, for example, in Refs.[11, 12]. A brief review of experimental prospects for studying photon induced interactions are summarized in Ref.[13].

As previously mentioned, the top quark is the heaviest known elementary particle which makes it an excellent candidate for new physics searches. Among top quark production channels, single top production has some special features that top pair production can not achieve: it offers a unique possibility of the direct measurement of  $V_{tb}$ , the Cabibbo-Kobayashi-Maskawa quark-mixing matrix (CKM), allowing non-trivial tests of the properties of this matrix in the SM[14, 15, 16]. In normal pp collision, single top produces mainly through two body s-channel (t-channel) single top in association with a b (light) quark,  $Wt$  channels and three body  $tbq'$  channel. Here we focus on the study of  $Wt$  channel. This channel is invisible at the Tevatron, however, it will be important at the LHC and even comparable to single top s-channel production. Even though, its cross section is almost a factor 100 smaller than the most dangerous background coming from the  $t\bar{t}$  process. This makes the measurement error of  $Wt$  process as large as  $\sim 41\%$  for an integrated luminosity of  $10 \text{ fb}^{-1}$  through normal pp collision[17]. Single top production can also proceed through  $\gamma p$  collisions mentioned above. This time through mainly  $Wt$  and  $tbq'$  channels. Compare these two channels, we find that cross section of  $Wt$  channel (order of  $\sim 1 \text{ pb}$ ), is much larger than that of  $tbq'$  channel (order of  $\sim 0.028 \text{ pb}$ ), and becomes the most important single top production channel at the  $\gamma p$  collision at the LHC. This is different from normal pp collision that  $tbq'$  production channel accounts for 44.2% (39%) of the total single top quark production cross section, while  $Wt$  channel stands only 28% (5%) at LHC (Tevatron)[18]. In contrast,  $Wt$  channel stands over 40% of the top quark photoproductions, since the top pair photoproduction has a cross section of only  $\sim 1.5 \text{ pb}$ . Enhancement of the ratio  $\sigma_{Wt}/\sigma_{t\bar{t}}$  might certainly be a good feature of related measurements through  $Wt$  channel.

First results on the measurement of the  $V_{tb}$  matrix element using  $Wt$  photoproduction are presented in Refs.[19, 20]. There comes the conclusion that the expected error on the measurement of  $V_{tb}$  is 16.9% for the semi-leptonic channel and 10.1% for the leptonic one after  $10 \text{ fb}^{-1}$  of integrated luminosity, while the expected uncertainty from the equivalent study based on partonic interactions is 14% [21] using the same integrated luminosity, showing that photoproduction is at least competitive with partonic-based studies and that the combination of both studies could lead to significant improvement of the error.

In addition to the  $V_{tb}$  measurement,  $Wt$  photoproduction can also be used to study the  $W$ - $t$ - $b$  vertex and test precisely the  $V$ - $A$  structure of the charged current weak interaction of the top quark. Anomalous measurement of this vertex may lead direct evidence of new physics beyond the SM. It may manifest itself via either loop effects or inducing non-SM weak interactions to introduce new single top production channels. Typical studies involve, i.e., measuring anomalous  $W$ - $t$ - $b$  coupling in  $ep$  collision[22, 23], in normal  $pp$  collision[24, 25, 26] as well as in  $\gamma p$  collision at the LHC[27]. Ref.[27] studies  $pp \rightarrow p\gamma p \rightarrow pW^{\pm}t + Y$  up to the leading order (LO) induced by anomalous  $W$ - $t$ - $b$  coupling. In this case, SM  $Wt$  photoproduction turns to its irreducible background. Moreover, a lot of studies are performed at the  $\gamma p$  colliders, i.e., testing anomalous gauge boson couplings [28, 29, 30, 31, 32, 33] or probing flavour changing neutral currents (FCNC) through single top photoproduction[34, 35], etc. In cases like these, SM  $Wt$  photoproduction turns to be a most important reducible background that needs precise measurement and analysis. Furthermore, determining  $Wt$  production cross sections and once compared with experiments, will provide a direct access to the bottom quark parton density in nucleons and help understand the nature of the  $b$  quark parton distribution function (PDF).

As a result, accurate theoretical predictions including higher order QCD corrections for  $Wt$  photoproduction are needed. NLO QCD corrections for  $Wt$  production in the normal  $pp$  collisions have already been well studied [36, 37, 38, 39, 40, 41, 42, 43]. In this paper, we present its production at the  $\gamma p$  collision for the first time, assuming a typical LHC multipurpose forward detector, including the NLO QCD corrections via the main reaction  $pp \rightarrow p\gamma p \rightarrow pW^{\pm}t + Y$ . Typically, we use the Five-Flavor-Number Schemes (5FNS) with

massless b quark mass assumption through the whole calculation. Our paper is organized as follow: we build the calculation framework in Section 2 including brief introduction to the Equivalent Photon Approximation (EPA), general inelastic photoproduction cross section, LO and QCD NLO Wt photoproductions. Section 3 is arranged to present the input parameters, cross checks and numerical results of our study. Finally we summarize our conclusions in the last section.

## 2 Calculation Framework

### 2.1 Equivalent Photon Approximation

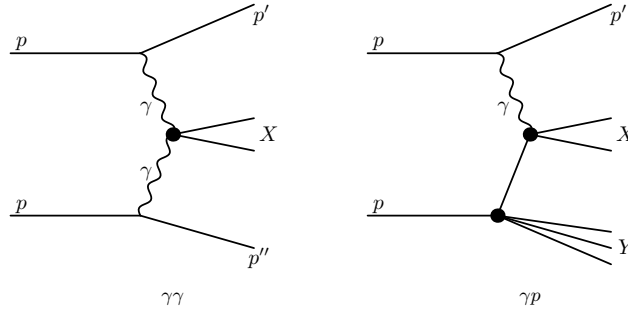


Figure 1: Generic diagrams for the photon induced production at the CERN LHC:  $pp \rightarrow p\gamma\gamma p \rightarrow pXp$  [left figure] and  $pp \rightarrow p\gamma p \rightarrow pXY$  [right figure].

In our paper, we focus on the discussion of photoproductions  $pp \rightarrow p\gamma p \rightarrow pXY$  through  $\gamma p$  collisions see Fig.1[right figure]. Photoproduction is a class of processes in which one of the two interacting protons is not destroyed during the collision but survive into the final state with additional particle (or particles) state(s). Protons of this kind are named intact or forward protons. The kinematics of a forward proton is often described by means of the reduced energy loss  $\xi$ , which is also defined as the forward detector acceptance:

$$\xi = \frac{\Delta E}{E} = \frac{E - E'}{E} \quad (1)$$

where  $E$  is the initial energy of the beam and  $s = 4E^2$  is the square of the centre-of-mass energy.  $E'$  is the energy after the interaction and  $\Delta E$  is the energy that the proton lost

in the interaction. Compare to the usual pp Deep Inelastic Scattering (DIS),  $\gamma\gamma$  and  $\gamma p$  collisions can provide more clean environment. Compare themselves,  $\gamma\gamma$  collisions can be cleaner than the  $\gamma p$  collisions. However,  $\gamma p$  collisions have higher energy and effective luminosity with respect to  $\gamma\gamma$  collisions.

Processes through  $\gamma\gamma$  or  $\gamma p$  interactions involve photon exchange with proton beams at the LHC which can be described by the appropriate framework of equivalent photon (or Weizsäcker-Williams) approximation (EPA) [44]. In the framework of EPA, emitted quasi-real photons from the protons have a low virtuality and scattered with small angles from the beam pipe. Therefore the emitters proton should also be scattered with a small angle and tagged by the forward detectors with some momentum fraction loss  $\xi$  given in Eq.(1). Higher  $\xi$  can be obtained with the closer installation of the forward detectors from the interaction points. The emitted quasi-real photons by the emitters protons with small angles show a spectrum of virtuality  $Q^2$  and the energy  $E_\gamma$ . This is described by the EPA which differs from the point-like electron (positron) case by taking care of the electromagnetic form factors in the equivalent photon spectrum and effective photon luminosity:

$$\frac{dN_\gamma}{dE_\gamma dQ^2} = \frac{\alpha}{\pi} \frac{1}{E_\gamma Q^2} \left[ \left(1 - \frac{E_\gamma}{E}\right) \left(1 - \frac{Q_{\min}^2}{Q^2}\right) F_E + \frac{E_\gamma^2}{2E^2} F_M \right] \quad (2)$$

with

$$Q_{\min}^2 = \left( \frac{M_{\text{inv}}^2 E}{E - E_\gamma} - M_p^2 \right) \frac{E_\gamma}{E}, \quad F_E = \frac{4M_p^2 G_E^2 + Q^2 G_M^2}{4M_p^2 + Q^2},$$

$$G_E^2 = \frac{G_M^2}{\mu_p^2} = \left(1 + \frac{Q^2}{Q_0^2}\right)^{-4}, \quad F_M = G_M^2, \quad Q_0^2 = 0.71 \text{ GeV}^2, \quad (3)$$

where  $\alpha$  is the fine-structure constant,  $E$  is the energy of the incoming proton beam. which is related to the quasi-real photon energy by  $E_\gamma = \xi E$ .  $M_p$  is the mass of the proton and  $M_{\text{inv}}$  is the invariant mass of the final state.  $\mu_p^2 = 7.78$  is the magnetic moment of the proton.  $F_E$  and  $F_M$  are functions of the electric and magnetic form factors given in the dipole approximation.

Many phenomenological studies on photon induced processes are summarized here involve: standard model productions [45], supersymmetry[46, 47], extra dimensions[48, 49,

50, 51], unparticle physics[52], top triangle moose model[53], gauge boson self-interactions [28, 29, 30, 31, 32, 33, 54, 55, 56, 57], neutrino electromagnetic properties[58, 59, 60], the top quark physics[19, 20, 27, 34, 35], dark matter searches[61] and triplet Higgs production[62], etc.

## 2.2 General $\gamma p$ Photoproduction Cross Section

We denote the general photoproduction processes at the LHC, no metter at LO or NLO level, as

$$pp \rightarrow p\gamma p \rightarrow p + \gamma + q/\bar{q}/g \rightarrow p + \underbrace{i + j + k + \dots}_X + Y \quad (4)$$

with  $q = u, d, c, s, b$  and  $i, j, k, \dots$  the final state particles. The hadronic cross section at the LHC can be converted by integrating  $\gamma + q/\bar{q}/g \rightarrow i + j + k + \dots$  over the photon ( $dN(x, Q^2)$ ), gluon and quark ( $G_{g,q/p}(x_2, \mu_f)$ ) spectra:

$$\begin{aligned} \sigma_{\gamma p} = \sum_{j=q,\bar{q},g} \int_{\frac{M_{\text{inv}}}{\sqrt{s}}}^{\sqrt{\xi_{\text{max}}}} 2zdz \int_{\text{Max}(z^2, \xi_{\text{min}})}^{\xi_{\text{max}}} \frac{dx_1}{x_1} \int_{Q_{\text{min}}^2}^{Q_{\text{max}}^2} \frac{dN_{\gamma}(x_1)}{dE_{\gamma}dQ^2} G_{g,q/p}\left(\frac{z^2}{x_1}, \mu_f\right) \\ \cdot \int \frac{1}{\text{avgfac}} \frac{|\mathcal{M}_n(\gamma j \rightarrow klm\dots, \hat{s} = z^2s)|^2}{2\hat{s}(2\pi)^{3n-4}} d\Phi_n, \end{aligned} \quad (5)$$

where  $x_1$  is the ratio between scattered quasi-real photons and incoming proton energy  $x_1 = E_{\gamma}/E$ .  $\xi_{\text{min}}(\xi_{\text{max}})$  are its lower (upper) limits which means that the forward detector acceptance satisfies  $\xi_{\text{min}} \leq \xi \leq \xi_{\text{max}}$ .  $x_2$  is the momentum fraction of the proton momentum carried by the gluon (quark). The quantity  $\hat{s} = z^2s$  is the effective c.m.s. energy with  $z^2 = x_1x_2$ .  $s = 4E^2$  mentioned above and  $M_{\text{inv}}$  is the total mass of the related final states.  $2z/x_1$  is the Jacobian determinant when transform the differentials from  $dx_1dx_2$  into  $dx_1dz$ .  $G_{g,q/p}(x, \mu_f)$  represent the gluon (quark) parton density functions,  $\mu_f$  is the factorization scale.  $f = \frac{dN}{dE_{\gamma}dQ^2}$  is the  $Q^2$  dependent relative luminosity spectrum present in Eq.(2).  $Q_{\text{max}}^2 = 2\text{GeV}^2$  is the maximum virtuality.  $\frac{1}{\text{avgfac}}$  is the product of the spin-average factor, the color-average factor and the identical particle factor.  $|\mathcal{M}_n|^2$  presents the squared  $n$ -particle matrix element and divided by the flux factor  $[2\hat{s}(2\pi)^{3n-4}]$ . The

$n$ -body phase space differential  $d\Phi_n$  and its integral  $\Phi_n$  depend only on  $\hat{s}$  and particle masses  $m_i$  due to Lorentz invariance:

$$\begin{aligned}\Phi_n(\hat{s}, m_1, m_2, \dots, m_n) &= \int d\Phi_n(\hat{s}, m_1, m_2, \dots, m_n) \\ &= \int \delta^4((p_i + p_j) - \sum_{k=1}^n p_k) \prod_{k=1}^n d^4 p_k \delta(p_k^2 - m_k^2) \Theta(p_k^0)\end{aligned}\quad (6)$$

with  $i$  and  $j$  denoting the incident particles and  $k$  running over all outgoing particles.

### 2.3 Wt Photoproduction at Leading Order

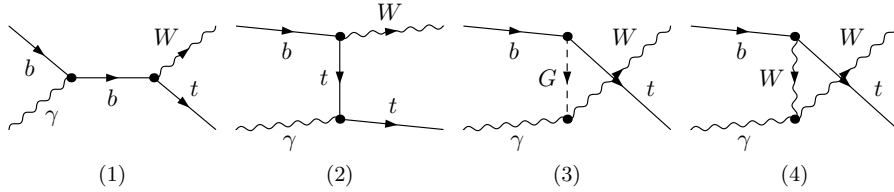


Figure 2: Tree level Feynman diagrams for  $\gamma b \rightarrow W^- t$  in the SM.

We denote the Wt photoproduction process as:

$$pp \rightarrow p\gamma p \rightarrow p\gamma(p_1)b(p_2) \rightarrow pW^-(p_3)t(p_4) + Y \quad (7)$$

where  $p_i$  are the particle four momentums. There are four LO Feynman diagrams for this partonic process as shown in Fig.2. There Fig.2(1) and Figs.2(2-4) are the s-channel and t-channel diagrams for the partonic process, respectively. Fig.2(3) include b-t-G vertex that can be safely omitted in the massless b quark assumption. We only consider the  $W^- t$  production while its charge-conjugate contribution is the same [41]. In order to describe the process  $\gamma(p_1)b(p_2) \rightarrow W^-(p_3)t(p_4)$  we choose the c.m.s. ( $\mathbf{p}_1 + \mathbf{p}_2 = 0$ ) with the momentum directed along z-axis. In c.m.s. the particle momentum read

$$\begin{aligned}p_1 &= \frac{\sqrt{\hat{s}}}{2}(e_1, 0, 0, e_{1z}), & p_3 &= \frac{\sqrt{\hat{s}}}{2}(e_3, e_{3x}, e_{3y}, e_{3z}) \\ p_2 &= \frac{\sqrt{\hat{s}}}{2}(e_2, 0, 0, e_{2z}), & p_4 &= \frac{\sqrt{\hat{s}}}{2}(e_4, e_{4x}, e_{4y}, e_{4z}).\end{aligned}\quad (8)$$

Here notation of  $e_{i/ix}$  equal  $p_{i/ix}/(\sqrt{\hat{s}}/2)$  and is needed in our following description.



The LO cross section for the partonic process  $\gamma b \rightarrow W^- t$  is obtained by using the following formula

$$\hat{\sigma}^{\text{LO}}(\hat{s}, \gamma b \rightarrow W^- t) = \frac{(2\pi)^4}{4|\mathbf{p}_1|\sqrt{\hat{s}}} \int \overline{\sum} |\mathcal{M}^{\text{LO}}|^2 d\Phi_2 \quad (9)$$

where  $d\Phi_2$  is the two-body phase-space element, and  $\mathbf{p}_1$  is the momentum of the initial photon in the c.m.s.. The integration is performed over the two-body phase space of the final particles  $W^- t$ . The summation is taken over the spins and colors of the initial and final states, and the bar over the summation indicates averaging over the intrinsic degrees of freedom of initial partons.

The LO total cross section for  $pp \rightarrow p\gamma p \rightarrow pW^- t$  can be expressed as

$$\begin{aligned} & \sigma^{\text{LO}}(pp \rightarrow p\gamma p \rightarrow pW^- t + Y) \\ &= \int_{\frac{M_{\text{inv}}}{\sqrt{s}}}^{\sqrt{\xi_{\text{max}}}} 2z dz \int_{\text{Max}(z^2, \xi_{\text{min}})}^{\xi_{\text{max}}} \frac{dx_1}{x_1} f_{\gamma/P_A}(x_1) G_{b/P_B}\left(\frac{z^2}{x_1}, \mu_f\right) \hat{\sigma}^{\text{LO}}(\gamma b \rightarrow W^- t, z^2 s, \mu_f, \mu_r) \\ &+ (A \leftrightarrow B). \end{aligned} \quad (10)$$

There  $G_{i/P_j}$ ,  $i=b$ ,  $j = A, B$  represent the PDFs of parton  $i$  in proton  $P_j$ ,  $\mu_f$  and  $\mu_r$  are the factorization and renormalization scales separately. Here we use  $f_{\gamma/P_A}(x_1)$  to take place of the  $\int_{Q_{\text{min}}^2}^{Q_{\text{max}}^2} \frac{dN_{\gamma}(x_1)}{dE_{\gamma}dQ^2}$  in Eq.(5) for simplicity. And we address here that during calculation, we use the  $\xi$ ,  $Q^2$  dependent form of Eq.(5).

## 2.4 Wt Photoproduction at QCD Next-to-Leading Order

### 2.4.1 General Description

We use the Five-Flavor-Number Scheme (5FNS) in our whole LO and QCD NLO calculations. As we see, at tree level in the 5FNS scheme the Wt photoproduction process consists of only one partonic subprocess, namely  $\gamma b \rightarrow W^- t$ , as illustrated in Fig.2. Indeed, Wt photoproduction can also be produced in the Four-Flavor-Number Scheme (4FNS) where the  $b$  quark is treated as massive and there is no  $b$  quark parton density is assumed in the initial state. In this scheme, the LO contribution starts from  $\gamma g \rightarrow W^- t \bar{b}$  with  $1b$  tagged in the final state. The first order of QCD corrections in 4FNS consist of virtual

one-loop corrections to the tree-level subprocesses as well as real corrections in the form of other two subprocesses with an additional radiated parton, namely  $\gamma g \rightarrow W^- t \bar{b} + g$  and  $\gamma q \rightarrow W^- t \bar{b} + \bar{q}$ . In the 4FNS scheme, b quark do not enter in the computation of the running of  $\alpha_s$  and the evolution of the PDFs. Finite  $m_b$  effects enter via power corrections of the type  $(m_b^2/Q^2)^n$  and logarithms of the type  $\log^n(m_b^2/Q^2)$  where  $Q$  stands for the hard scale of the process. At the LHC, typically  $(m_b/Q) \ll 1$  and power corrections are suppressed, while logarithms, both of initial and final state nature, could be large. These large logarithms could in principle spoil the convergence of fixed order calculations and a resummation could be required. Up to NLO accuracy those potentially large logarithms,  $\log(m_b/Q)$ , are replaced by  $\log(p_{T,b}^{\min}/Q)$  with  $m_b \ll p_{T,b}^{\min} \leq Q$  and are less significant numerically. As can be seen, the difference between adopting the 5FNS and 4FNS is the ordering of the perturbative series for the production cross section. In the 4FNS the perturbative series is ordered strictly by powers of the strong coupling  $\alpha_s$ , while in the 5FNS the introduction of the b quark PDF allows to resum terms of the form  $\alpha_s^n \log(\mu^2/m_b^2)^m$  at all orders in  $\alpha_s$ . If all orders in perturbation theory were taken into account, these two schemes are identical in describing logarithmic effects. But the way of ordering in the perturbative expansion is different and at any finite order the results might be different. Many works have been done in the comparison of the 5FNS and 4FNS Schemes, see Refs.[63, 64, 65, 66, 67, 68, 69], etc. A latest comparison in the 4FNS and 5FNS schemes in Ref.[70] present that being often the effects of resummation very mild, 4FNS calculations can be put to use, on the other hand, for 5FNS schemes, i.e., can typically provide quite accurate predictions for total rates and being simpler, in some cases allow the calculations to be performed at NNLO. We address the interesting of considering both schemes while here we use 5FNS in our calculation. Even in 5FNS, it will be interesting to consider two schemes [71, 72]: one is the massless b quark scheme where we drop the mass of b quark during calculation while the other is the massive b quark scheme where we retain it everywhere.

In our paper, we adopt the 5FNS scheme with the massless b quark assumption. In this case, the first order of QCD corrections to the  $pp \rightarrow p\gamma p \rightarrow pW^- t + Y$  consist of:

- The QCD one-loop virtual corrections to the partonic process  $\gamma b \rightarrow W^- t$ .
- The contribution of the real gluon radiation partonic process  $\gamma b \rightarrow W^- t + g$ .
- The contribution of the real b-quark emission partonic process  $\gamma g \rightarrow W^- t + \bar{b}$ .
- The corresponding contributions of the PDF counterterms.

We use the dimensional regularization method in  $D = 4 - 2\epsilon$  dimensions to isolate the ultraviolet (UV) and infrared (IR) singularities. In massless b quark scheme, we split each collinear counter-term of the PDF,  $\delta G_{b/P}(x, \mu_f)$  (P=proton), into two parts: the collinear gluon emission part  $\delta G_{b/P}^{\text{gluon}}(x, \mu_f)$  and the collinear b quark emission part  $\delta G_{b/P}^{\text{quark}}(x, \mu_f)$ . The analytical expressions are presented as follows

$$\delta G_{b/P}(x, \mu_f) = \delta G_{b/P}^{\text{gluon}}(x, \mu_f) + \delta G_{b/P}^{\text{quark}}(x, \mu_f) \quad (11)$$

with

$$\begin{aligned} \delta G_{b/P}^{\text{gluon}} &= \frac{1}{\epsilon} \left[ \frac{\alpha_s}{2\pi} \frac{\Gamma(1-\epsilon)}{\Gamma(1-2\epsilon)} \left( \frac{4\pi\mu_r^2}{\mu_f^2} \right)^\epsilon \right] \int_x^1 \frac{dz}{z} P_{bb}(z) G_{b/P}\left(\frac{x}{z}, \mu_f\right) \\ \delta G_{b/P}^{\text{quark}} &= \frac{1}{\epsilon} \left[ \frac{\alpha_s}{2\pi} \frac{\Gamma(1-\epsilon)}{\Gamma(1-2\epsilon)} \left( \frac{4\pi\mu_r^2}{\mu_f^2} \right)^\epsilon \right] \int_x^1 \frac{dz}{z} P_{bg}(z) G_{g/P}\left(\frac{x}{z}, \mu_f\right) \end{aligned} \quad (12)$$

and the explicit expressions for the splitting functions  $P_{ij}(z)$ , ( $ij = bb, bg$ ) can be found in Ref.[73].

### 2.4.2 Virtual

The amplitude at the QCD one-loop level for the partonic process  $\gamma b \rightarrow W^- t$  in the SM contains the contributions of the self-energy, vertex, box and counter-term graphs which are shown in Fig.3(1)-(18). Same as the leading level that diagrams include b-t-G vertex that can be safely omitted in the massless b quark scheme. Even in the massive b quark scheme, their contributions are also quite small.

To remove the UV divergences, we need to renormalize the mass of the quarks and the wave function of the quark fields. In the massless b quark assumption we introduce

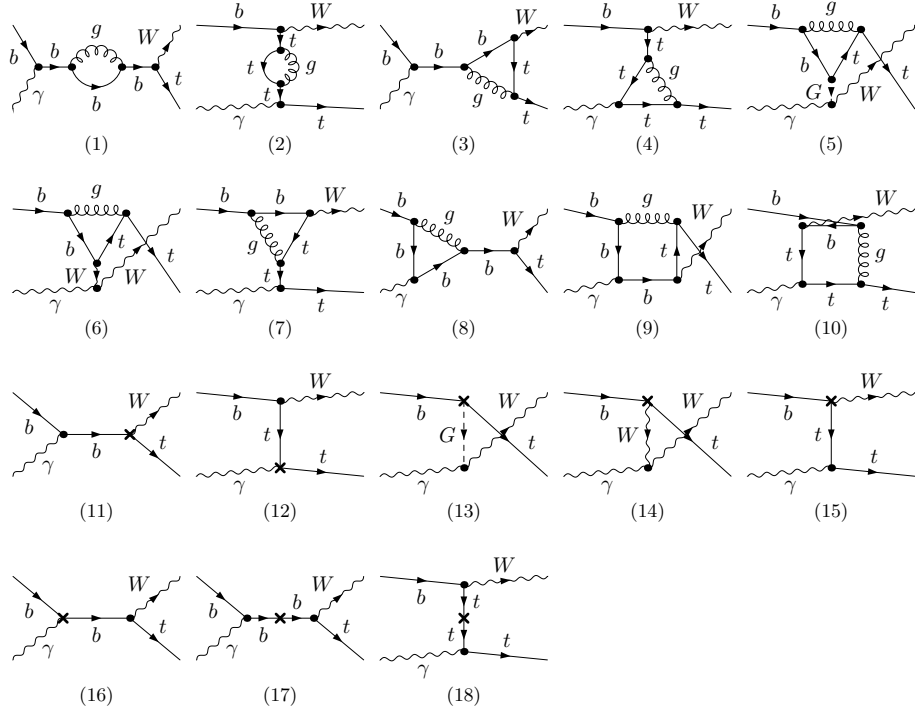


Figure 3: QCD one loop Feynman diagrams for  $\gamma b \rightarrow W^- t$  in the SM.

the following renormalization constants:

$$\begin{aligned}\psi_{b(t)}^{0,L,R} &= \left(1 + \delta Z_{\psi_{b(t)}}^{L,R}\right)^{\frac{1}{2}} \psi_{b(t)}^{L,R}, \\ m_t^0 &= m_t + \delta m_t,\end{aligned}\tag{13}$$

where  $m_t$  are the top-quark mass.  $\psi_{b(t)}^{L,R}$  denote the fields of bottom (top) quark. For the masses and wave functions of the fields are renormalized in the on-shell scheme and the relevant counter-terms are expressed as

$$\begin{aligned}\delta Z_{\psi_t}^{L,R} &= -\frac{\alpha_s}{4\pi} C_F \left[ \Delta_{UV} + 2\Delta_{IR} + 4 + 3\ln\left(\frac{\mu_r^2}{m_t^2}\right) \right], \\ \frac{\delta m_t}{m_t} &= -\frac{\alpha_s}{4\pi} C_F \left[ 3\Delta_{UV} + 4 + 3\ln\left(\frac{\mu_r^2}{m_t^2}\right) \right],\end{aligned}\tag{14}$$

with  $C_F = \frac{4}{3}$ ,  $\Delta_{UV(IR)} = \frac{1}{\epsilon_{UV(IR)}} \Gamma(1 + \epsilon_{UV(IR)}) (4\pi)^{\epsilon_{UV(IR)}}$  refer to the UV(IR) divergences. For massless b quark, there is no need to renormalize the mass of bottom and we use modified minimal subtraction ( $\overline{MS}$ ) scheme for b field as:

$$\delta Z_{\psi_b}^{L,R} = -\frac{\alpha_s}{4\pi} C_F [\Delta_{UV} - \Delta_{IR}].\tag{15}$$

UV singularities are regulated by adding renormalization part to the virtual corrections only leaving IR singularities that will be removed by combining the real emission corrections. We calculate the virtual one-loop corrections ( $\sigma^V$ ) using a Feynman diagram approach based on FeynArts, FormCalc and our modified LoopTools (FFL)[74, 75, 76] packages. Tensor one loop integrals are checked with OneLoop[77] and QCDLoop[78] packages.

### 2.4.3 Parton Radiation

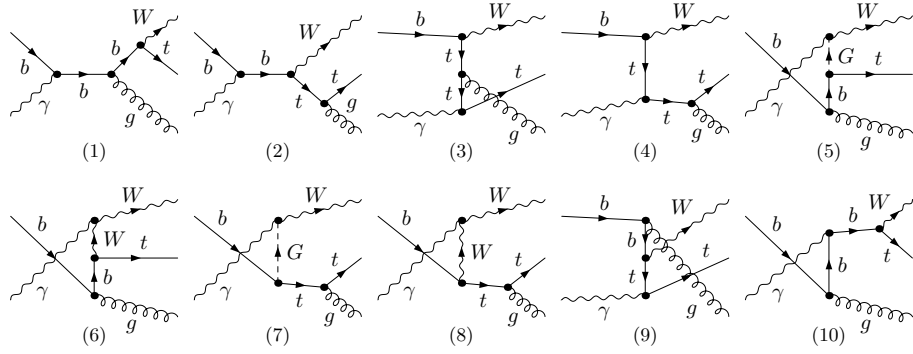


Figure 4: The tree parton level Feynman diagrams for the real gluon emission subprocess  $\gamma b \rightarrow W^- t g$  related to Eq.(16).

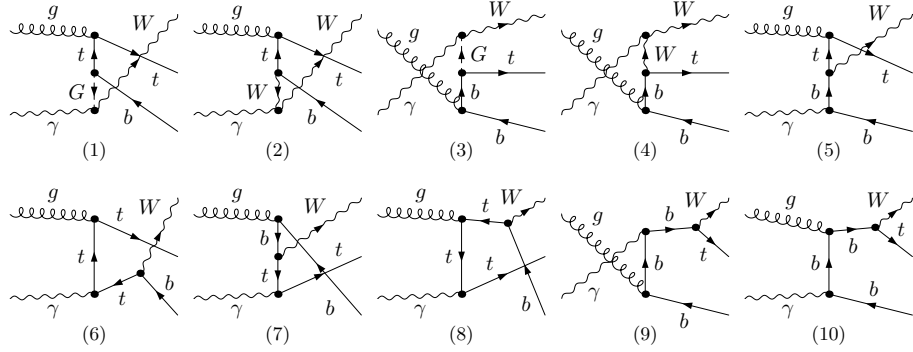


Figure 5: The tree parton level Feynman diagrams for the real light-(anti)quark emission subprocess  $\gamma g \rightarrow W^- t \bar{b}$  related to Eq.(17).

The first order of QCD corrections also consist of the real corrections in the form of

other two subprocesses with an additional radiated parton, namely gluon emission and real (anti) quark emission presented as

$$\gamma(p_1)b(p_2) \rightarrow W^-(p_3)t(p_4)g(p_5) \quad (16)$$

$$\gamma(p_1)g(p_2) \rightarrow W^-(p_3)t(p_4)\bar{b}(p_5) \quad (17)$$

with Feynman diagrams depicted in Fig.4 and Fig.5, respectively.

In the massless b quark scheme, singularities associated with initial state collinear gluon emission are absorbed into the definition of the PDFs, see in Eq.(12). We employ the  $\overline{\text{MS}}$  scheme for the parton distribution functions. Similar to the virtual part, we utilize dimensional regularization (DR) to control the singularities of the radiative corrections, which are organized using the two cutoff phase space slicing (TCPSS) method[73]. Since we treat the b quark as massless, there is collinear IR singularity which is regularized by  $1/\epsilon$  in the DR scheme. This term is canceled by the corresponding contribution in the b quark PDF counterterm, in other words, absorbed by the b quark PDF. This cancellation has been checked both analytically and numerically, therefore, avoid double counting problem. We adopt TCPSS to isolate the IR singularities by introducing two cutoff parameters  $\delta_s$  and  $\delta_c$ . An arbitrary small  $\delta_s$  separates the three-body final state phase space into two regions: the soft region ( $E_5 \leq \delta_s \sqrt{\hat{s}}/2$ ) and the hard region ( $E_5 > \delta_s \sqrt{\hat{s}}/2$ ). The  $\delta_c$  separates hard region into the hard collinear (HC) region and hard noncollinear ( $\overline{\text{HC}}$ ) region. The criterion for separating the HC region is described as follows: the region for real gluon/light quark emission with  $\hat{s}_{15}$  (or  $\hat{s}_{25}$ )  $< \delta_c \hat{s}$  (where  $\hat{s}_{ij} = (p_i + p_j)^2$ ) is called the HC region. Otherwise it is called the  $\overline{\text{HC}}$  region.

At QCD NLO, some of the contributions representing the emission of an additional parton require special attention. For example, when we calculate the remain part in real radiation corrections  $\gamma g \rightarrow Wtb$  (Eq.17), appropriate crossing of the diagrams shown in Fig.5 should be included. Some of the diagrams which produce a final state consisting of a W, an on-shell top quark and a b quark are particularly problematic. During phase space integration, one need to integrate over the region  $M_{Wb}^2 = (p_W + p_b)$ . If in this case, a resonant t propagator (with flowing momentum equal or close to  $p_W + p_b$ ) is

encountered, a divergence will arise. Actually these diagrams can be interpreted as the production of a  $t\bar{t}$  pair at LO, with subsequent decay of the top into a  $Wb$  system. This is the well known interference between  $Wt$  and  $t\bar{t}$  production, namely doubly resonant. Such resonant becomes extremely large in certain phase space region and renders the perturbative computation of the  $Wt$  cross section meaningless, thus should be preferable excluded from the NLO corrections to the  $Wt$  process.

Several approaches have been outlined in the literature, i.e., making a cut on the invariant mass of the  $Wb$  system to prevent the  $t$  propagator from becoming resonant [18], subtracting the contribution from the resonant diagrams so that no on-shell piece remains [79, 80], bottom quark PDF method, technically, perform calculation of the  $Wt$  process by applying a veto on the  $p_T$  of the additional  $b$  quark that appears at next-to-leading order aids the separation of this process from doubly-resonant  $t\bar{t}$  production [42], etc [41, 81]. Here in our case we use the PROSPINO scheme [82] which is defined as a replacement of the Breit-Wigner propagator

$$\frac{|\mathcal{M}|^2(s_{Wb})}{(s_{Wb} - m_t^2)^2 + m_t^2 \Gamma_t^2} \rightarrow \frac{|\mathcal{M}|^2(s_{Wb})}{(s_{Wb} - m_t^2)^2 + m_t^2 \Gamma_t^2} - \frac{|\mathcal{M}|^2(m_t^2)}{(s_{Wb} - m_t^2)^2 + m_t^2 \Gamma_t^2} \Theta(\hat{s} - 4m_t^2) \Theta(m_t - m_W). \quad (18)$$

This subtraction scheme helps to avoid double counting and to not artificially ruin the convergence of the perturbative QCD description of these production channels with the remove of on-shell particle contributions from the associated production. This scheme has be done in some other refs like [83, 84, 85, 86], etc.

Some attention should be paid to the light-(anti)quark emission subprocess, see Figs.5(5) and Fig.5(10). Contributions from these two diagrams can be considered as part of the NLO EW corrections to the LO process  $pp \rightarrow gb \rightarrow Wt$  through normal  $pp$  collision. Since we concentrate on the photoproduction of  $pp \rightarrow p\gamma p \rightarrow pW^-t$  where forward protons are considered, the  $pp \rightarrow gb \rightarrow Wt$  and its full NLO EW corrections are not taken into account. Then, the subprocesses in Figs. 5(5) and 5(10) are defined applying a small  $p_T$  cut on the tagged  $b$  quark, which regularize the collinear splitting of the photon into a  $b\bar{b}$  pair. Indeed, the choice of specific kinematical cuts to select events in the forward re-

gion (small  $p_T$  cut applied on the tagged b quark) forces the contributions from these two diagrams to be quite small. Thus, even when one is forced to consider them as part of the NLO QCD corrections to the  $pp \rightarrow p\gamma p \rightarrow pWt$  production process, their contribution results for only but a tiny theoretical uncertainty.

Then the cross section for each of the real emission partonic processes can be written as  $\hat{\sigma}^R = \hat{\sigma}^S + \hat{\sigma}^H = \hat{\sigma}^S + \hat{\sigma}^{HC} + \hat{\sigma}^{\overline{HC}}$ . After integrating over the photon and quark spectra, we get the real contributions as  $\sigma^R = \sigma^S + \sigma^{HC} + \sigma^{\overline{HC}}$ .

#### 2.4.4 Total QCD NLO Cross Section

After combining all the contributions that are mentioned before, the UV, IR singularities in our final total cross section

$$\begin{aligned}\sigma^{\text{NLO}} &= \sigma^{\text{LO}} + \sigma^{\text{V}} + \sigma^{\text{R}} \\ &= \sigma^{\text{LO}} + \sigma^{\text{V}} + \sigma^{\text{S}} + \sigma^{\text{HC}} + \sigma^{\overline{\text{HC}}}\end{aligned}\quad (19)$$

are exactly cancelled. The logarithmic dependence on the arbitrary small cutoff parameters  $\delta_s$  and  $\delta_c$  are then cancelled (but power-like terms survive). These cancelations can be verified numerically in our numerical calculations. The final results of the total QCD NLO cross section in the 5FNS scheme can be expressed as:

$$\begin{aligned}&\sigma^{\text{NLO}}(pp \rightarrow p\gamma p \rightarrow pW^-t + Y) \\ &= \int_{\frac{M_{\text{inv}}}{\sqrt{s}}}^{\sqrt{\xi_{\text{max}}}} 2zdz \int_{\text{Max}(z^2, \xi_{\text{min}})}^{\xi_{\text{max}}} \frac{dx_1}{x_1} f_{\gamma/P_A}(x_1) \{ G_{b/P_B}(\frac{z^2}{x_1}, \mu_f) [\hat{\sigma}^{\text{LO}} + \hat{\sigma}^{\text{V}} + (F^{\text{soft}} + F^{\text{hc}}) \hat{\sigma}^{\text{LO}} \\ &\quad + (F^1 + F^2) \hat{\sigma}^{\text{LO}} + \hat{\sigma}_g^{\overline{\text{HC}}}] + G_{g/P_B}(\frac{z^2}{x_1}, \mu_f) \hat{\sigma}_b^{\overline{\text{HC}}} \} + (A \leftrightarrow B).\end{aligned}\quad (20)$$

Here  $F^{\text{soft}}$  and  $F^{\text{hc}}$  are the factors contain soft and collinear singularities as well as finite terms.  $F^{1,2}$  are the factors that finite. In the massless b quark assumption, there analytical expression are

$$F^{\text{soft}} + F^{\text{hc}} = C_F \frac{\alpha_s}{2\pi} \left( \frac{A_2}{\epsilon^2} + \frac{A_1}{\epsilon} + A_0 \right) \quad (21)$$



with

$$\begin{aligned}
A_2 &= 1 \\
A_1 &= \ln \frac{\mu_r^2}{\hat{s}} - \ln \frac{(e_4 - e_{4z})^2}{e_4^2 - e_{4z}^2 - e_{4x}^2} + \frac{5}{2} \\
A_0 &= \frac{1}{2} \ln^2 \frac{\mu_r^2}{\hat{s}} - 2 \ln \delta_s \ln \frac{\mu_r^2}{\hat{s}} + 2 \ln^2 \delta_s - 2 \ln \delta_s + \ln \frac{\mu_r^2}{\hat{s}} - \ln \frac{\mu_r^2}{\hat{s}} \ln \frac{(e_4 - e_{4z})^2}{e_4^2 - e_{4z}^2 - e_{4x}^2} \\
&+ 2 \ln \delta_s \ln \frac{(e_4 - e_{4z})^2}{e_4^2 - e_{4z}^2 - e_{4x}^2} + \frac{e_4}{\sqrt{e_{4z}^2 + e_{4x}^2}} \ln \frac{e_4 + \sqrt{e_{4z}^2 + e_{4x}^2}}{e_4 - \sqrt{e_{4z}^2 + e_{4x}^2}} \\
&+ \ln^2 \frac{e_4 - \sqrt{e_{4z}^2 + e_{4x}^2}}{e_4 - e_{4z}} - \frac{1}{2} \ln^2 \frac{e_4 + \sqrt{e_{4z}^2 + e_{4x}^2}}{e_4 - \sqrt{e_{4z}^2 + e_{4x}^2}} \\
&+ 2 \text{Li}_2 \left( \frac{e_{4z} - \sqrt{e_{4z}^2 + e_{4x}^2}}{e_4 - \sqrt{e_{4z}^2 + e_{4x}^2}} \right) - 2 \text{Li}_2 \left( \frac{-e_{4z} - \sqrt{e_{4z}^2 + e_{4x}^2}}{e_4 - e_{4z}} \right)
\end{aligned} \tag{22}$$

and

$$\begin{aligned}
F^1 &= \frac{\alpha_s}{2\pi} \int_{\frac{z^2}{x_1}}^{1-\delta_s} \frac{dy}{y} G_{b/P_B} \left( \frac{z^2}{x_1 y}, \mu_f \right) \left[ C_F \frac{1+y^2}{1-y} \ln \left( \delta_s \frac{1-y}{y} \right) \frac{\hat{s}}{\mu_f^2} + (1-y) \right] \\
F^2 &= \frac{\alpha_s}{2\pi} \int_{\frac{z^2}{x_1}}^1 \frac{dy}{y} G_{g/P_B} \left( \frac{z^2}{x_1 y}, \mu_f \right) \left[ -\frac{1}{2} (y^2 + (1-y)^2) \ln \left( \delta_s \frac{1-y}{y} \right) \frac{\hat{s}}{\mu_f^2} + y(1-y) \right].
\end{aligned}$$

Notations of  $e_{i/ix}$  can be found in Eq.(8). The dilogarithm function  $\text{Li}_2(x)$  is defined in Ref[87]. Technical details can be found in Ref[73, 88].

## 3 Numerical Results

### 3.1 Input Parameters

We take the input parameters as  $M_p = 0.938272046$  GeV,  $\alpha_{ew}(m_Z^2)^{-1}|_{\overline{\text{MS}}} = 127.918$ ,  $m_Z = 91.1876$  GeV,  $m_W = 80.385$  GeV[89] and we have  $\sin^2 \theta_W = 1 - (m_W/m_Z)^2 = 0.222897$ . The PDFs are taken from the LHAPDF package[90]. We adopt the CTEQ6L1 and CTEQ6M PDFs[91] for the LO and QCD higher order calculations, separately. The strong coupling constant  $\alpha_s(\mu)$  is determined by the QCD parameter  $\Lambda_5^{\text{LO}} = 165$  MeV for the CTEQ6L1 and  $\Lambda_5^{\overline{\text{MS}}} = 226$  MeV for the CTEQ6M, respectively. For simplicity we set the factorization scale and the renormalization scale being equal (i.e.,  $\mu = \mu_f = \mu_r$ ) and

take  $\mu = \mu_0 = (m_t + m_W)/2$  in default unless otherwise stated. Throughout this paper, we set the quark masses as  $m_u = m_d = m_c = m_s = m_b = 0$ , The top quark pole mass is set to be  $m_t = 173.5$  GeV. The colliding energy in the proton-proton center-of-mass system is assumed to be  $\sqrt{s} = 14$  TeV at future LHC. We adopt BASES[92] to do the phase space integration. The CKM matrix elements are set as unit. The decay of the top quark is expected to be dominated by the two-body channel  $t \rightarrow W^- b$  and the total decay width of the top quark is approximately equal to the decay width of  $t \rightarrow W^- b$ . Neglecting terms of order  $m_b^2/m_t^2$ ,  $\alpha_s$ , and  $(\alpha_s/\pi)m_W^2/m_t^2$ , the width predicted in the SM at NLO is:

$$\Gamma_t = \frac{\alpha_{\text{ew}} m_t^3}{16 m_W^2 s_W^2} \left(1 - \frac{m_W^2}{m_t^2}\right)^2 \left(1 + \frac{2m_W^2}{m_t^2}\right) \left[1 - \frac{2\alpha_s}{3\pi} \left(\frac{2\pi^2}{3} - \frac{5}{2}\right)\right]. \quad (23)$$

By taking  $\alpha_{\text{ew}}(m_Z^2)^{-1}|_{\overline{\text{MS}}} = 127.918$  and  $\alpha_s(m_t^2) = 0.1079$ , we obtain  $\Gamma_t = 1.41595$  GeV. Based on the forward proton detectors to be installed by the CMS-TOTEM and the ATLAS collaborations we choose the detected acceptances to be

- CMS-TOTEM forward detectors with  $0.0015 < \xi_1 < 0.5$
- CMS-TOTEM forward detectors with  $0.1 < \xi_2 < 0.5$
- AFP-ATLAS forward detectors with  $0.0015 < \xi_3 < 0.15$

which we simply refer to  $\xi_1$ ,  $\xi_2$  and  $\xi_3$ , respectively. During calculation we use  $\xi_1$  in default unless otherwise stated. Note here we do not consider the decay of the heavy final states as well as the survival probability in the  $\gamma p$  collision or simply taken to be unit.

## 3.2 Cross Checks

Before presenting the numerical predictions, several cross checks should be done.

- First, during the calculation of the tensor one loop integrals, we use our modified LoopTools and cross check with OneLoop[77] and QCDDLoop[78] packages. We can get exactly the same results in each phase space point.

- Second, when do the phase space integration we use BASES[92] and cross check independently with Kaleu[93] especially for the hard emission contributions. We can get the same integrated results within the error.
- Third, the UV and IR safeties should be verified numerically after combining all the contributions at the NLO QCD loop level. To check this, we display enough random phase space point as well as the cancellation for different divergent parameters, see in Table.1 corresponding to 5FNS massless b quark scheme. One thing that should be emphasized is  $\hat{\sigma}^V$  should include the counter-term contributions as well as the soft and collinear singularity terms coming from the real emissions. We implement this into our monte carlo codes which provide an automatic check of the dependence on these divergence parameters. We can see the UV and IR divergence can be canceled at high precision level in all the phase space thus leading the continuance of our following calculation.

$pp \rightarrow p\gamma p \rightarrow p\gamma(p_1)b(p_2) \rightarrow pW(p_3)t(p_4) + Y$ with $m_b = 0$ [pb]			
$p_1=(218.59020657143321 \ 0 \ 0 \ 218.59020657143321)$			
$p_2=(218.59020657143321 \ 0 \ 0 \ -218.59020657143321)$			
$p_3=(191.55273981365957 \ 148.54834482485680 \ 0 \ 90.355371477931513)$			
$p_4=(245.62767332920686 \ -148.54834482485680 \ 0 \ -90.355371477931513)$			
$\frac{1}{\epsilon_{UV}} = \frac{1}{\epsilon_{IR}^2} = \frac{1}{\epsilon_{IR}} = 0$	$\hat{\sigma}^{LO} = 0.7990$	$\hat{\sigma}^V = \hat{\sigma}^0 = 2.2672370626972782$	
$\frac{1}{\epsilon_{UV}} = \frac{1}{\epsilon_{IR}^2} = \frac{1}{\epsilon_{IR}} = 10^{10}$	$\hat{\sigma}^{LO} = 0.7990$	$\hat{\sigma}^V = \hat{\sigma}^0 + 7 \times 10^{-17}$	

Table 1: The UV and IR divergence cancelation at one given random phase space point for the loop contribution for  $pp \rightarrow p\gamma p \rightarrow p\gamma(p_1)b(p_2) \rightarrow pW(p_3)t(p_4) + Y$  with  $m_b = 0$ .

- Fourth, since the total cross section is independent of the soft cutoff  $\delta_s$  ( $= \Delta E_g/E_b$ ,  $E_b = \sqrt{\hat{s}}/2$ ) and the collinear cutoff  $\delta_c$ , we display their values for  $pp \rightarrow p\gamma p \rightarrow pWt$  versus the cutoff  $\delta_s$ , where we take  $\delta_c = \delta_s/100$ . Both  $\delta_s$  and  $\delta_c$  dependence should be

$\delta_s$ dependence for $\sigma(\text{pp} \rightarrow \text{p}\gamma\text{p} \rightarrow \text{pWt} + \text{Y})[\text{pb}]$ with $m_b = 0$			
$\delta_s = 100\delta_c$	$\sigma^{\text{LO}}$	$\sigma^{\text{NLO}}$	$\Delta = \sigma^{\text{NLO}} - \sigma^{\text{LO}}$
$1 \times 10^{-3.0}$	1.14255073	1.34824330	0.20569257
$1 \times 10^{-3.5}$	1.14255073	1.34968444	0.20713371
$1 \times 10^{-4.0}$	1.14255073	1.34910699	0.20655626
$1 \times 10^{-4.5}$	1.14255073	1.34921708	0.20666635
$1 \times 10^{-5.0}$	1.14255073	1.34937836	0.20682763
$1 \times 10^{-5.5}$	1.14255073	1.35015998	0.20760925
$1 \times 10^{-6.0}$	1.14255073	1.34720592	0.20465519

Table 2: The  $\delta_s$  dependence of the loop induced QCD correction to the integrated cross section for the  $\text{pp} \rightarrow \text{p}\gamma\text{p} \rightarrow \text{pWt} + \text{Y}$  with  $m_b = 0$  at the  $\sqrt{s} = 14$  TeV LHC where we set  $\delta_c = \delta_s/100$ . The detector acceptance here is chosen to be  $0.0015 < \xi_1 < 0.5$ .

checked. Some of the results are listed in Table.2. The detector acceptance here is chosen to be  $0.0015 < \xi_1 < 0.5$ . It is shown clearly that the NLO QCD correction does not depend on the arbitrarily chosen values of  $\delta_s$  and  $\delta_c$  within the calculation errors. In the further numerical calculations, we fix  $\delta_s = 10^{-4}$  and  $\delta_c = \delta_s/100$ .

### 3.3 Scale dependence for different forward detector acceptances

We present the scale- $\mu$  dependence of the LO and QCD NLO corrected cross sections for  $\text{pp} \rightarrow \text{p}\gamma\text{p} \rightarrow \text{pWt} + \text{Y}$  for the CMS-TOTEM forward detectors with  $0.0015 < \xi_1 < 0.5$  in the left panel of Fig.6. Scale- $\mu$  varies from  $\mu_0/8$  to  $2\mu_0$  with  $\mu_0 = (m_W + m_t)/2$ . In the figure, solid lines with plus sign points present the LO predictions. Its cross section varies from 0.5772 pb to 1.2717 pb with the scale- $\mu$  varies from  $\mu_0/8$  to  $2\mu_0$ . The deviation is as large as 0.6945 pb shows some dependence on the scale. We use dotted line with times sign to present the QCD NLO corrected cross section in the 5FNS massless b quark

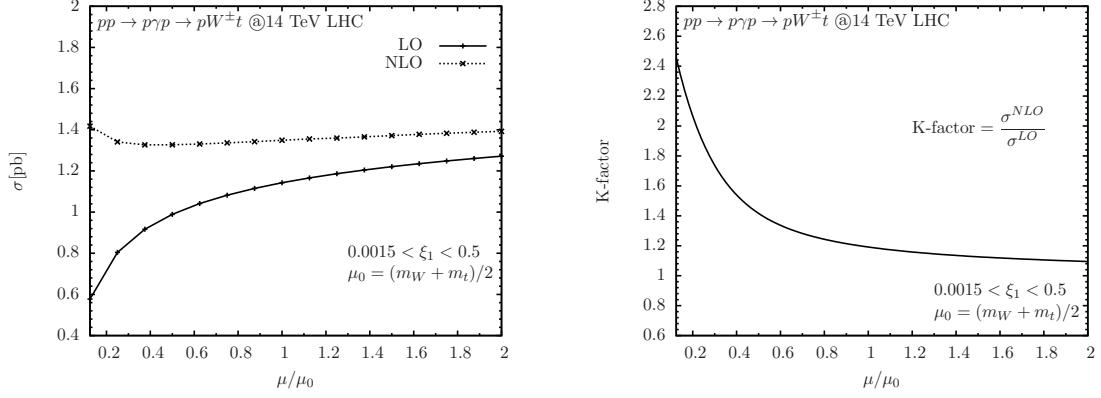


Figure 6: The scale- $\mu$  dependence of the LO and QCD NLO corrected cross sections [left panel] and K-factor [right panel] for  $pp \rightarrow p\gamma p \rightarrow pW^\pm t + Y$  at the  $\sqrt{s} = 14$  TeV LHC with  $\mu_0 = (m_W + m_t)/2$ ,  $\delta_s = 10^{-4}$  and  $\delta_c = \delta_s/100$ . The experimental acceptance here is chosen to be  $0.0015 < \xi_1 < 0.5$  for the CMS-TOTEM forward detectors.

scheme. The NLO cross section changes from 1.4175 pb to 1.3922 pb with the deviation only 0.0253 pb. We can see that if the QCD NLO corrections are taken into account, much better scale- $\mu$  independence can be obtained and the factorization/renormalization scale uncertainty can be reduced. In the right panel of Fig.6, we show the K-factor of the QCD NLO contribution as function of scale- $\mu$ . K-factor is defined as  $\sigma^{\text{NLO}}/\sigma^{\text{LO}}$ . We see that K-factor is large and sensitive in the small  $\mu$  range while insensitive at the large  $\mu$ . Typical results of the K-factor are 2.4557, 1.3415, 1.1808 and 1.0947 for  $\mu_0/8$ ,  $\mu_0/2$ ,  $\mu_0$  and  $2\mu_0$ , respectively.

In Fig.7, the scale- $\mu$  dependence of the LO cross section, QCD NLO corrected cross section and K-factor are depicted in the left and right panel for the CMS-TOTEM forward detectors with  $0.1 < \xi_2 < 0.5$ . Same as in Fig.6, we use solid lines with plus sign points present the LO predictions and dotted line with times sign to present the QCD NLO corrected cross section, respectively. When  $\mu$  varies from  $\mu_0/8$  to  $2\mu_0$ , their cross sections change from 0.2097(0.5485) pb to 0.5401(0.5601) pb with their ratio equal 2.58 (1.02). Still we can see the NLO predictions can reduce the factorization/renormalization scale uncertainty corresponding to the LO prediction. We see NLO correction shows much

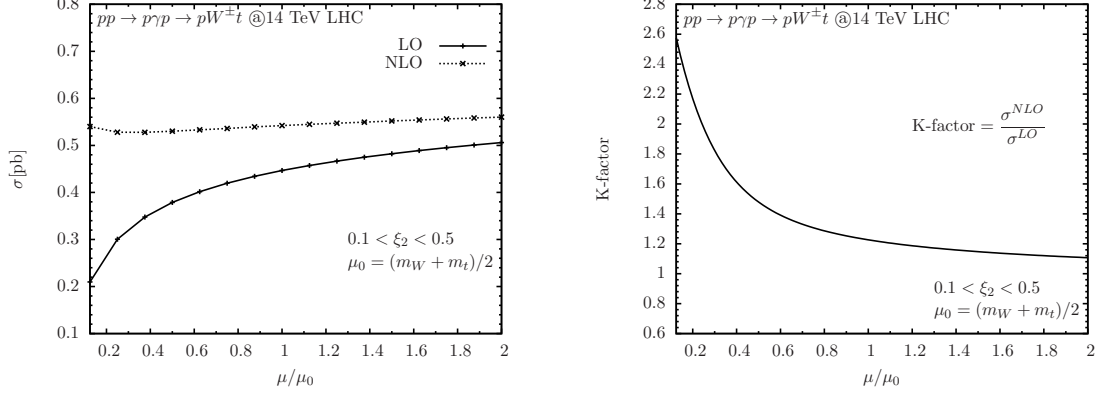


Figure 7: The scale- $\mu$  dependence of the LO and QCD NLO corrected cross sections [left panel] and K-factor [right panel] for  $pp \rightarrow p\gamma p \rightarrow pWt + Y$  at the  $\sqrt{s} = 14$  TeV LHC with  $\mu_0 = (m_W + m_t)/2$ ,  $\delta_s = 10^{-4}$  and  $\delta_c = \delta_s/100$ . The experimental acceptance here is chosen to be  $0.1 < \xi_2 < 0.5$  for the CMS-TOTEM forward detectors.

better scale independence through the whole range  $[\mu_0/8, 2\mu_0]$ . Compare the results with  $0.0015 < \xi_1 < 0.5$ , we see for  $0.1 < \xi_2 < 0.5$ , in the whole range, both the LO and QCD NLO corrected cross sections are smaller, less than half of than that of  $0.0015 < \xi_1 < 0.5$ .

For the AFP-ATLAS forward detectors with  $0.0015 < \xi_3 < 0.15$ , the cross section for the LO and QCD NLO prediction are close to that of  $0.0015 < \xi_1 < 0.5$ , see Fig.8. Behavior of the cross sections and K-factor on the scale- $\mu$  dependence are the same. In this case their cross sections change from 0.4447(1.0717) pb to 0.9454(1.0297) pb with their ratio equal 2.13 (0.96) when  $\mu$  varies from  $\mu_0/8$  to  $2\mu_0$ . We conclude again that the QCD NLO corrections can reduce the factorization/renormalization scale uncertainty. Finally we summary the K-factor for typical value of  $\mu$  in Table.3 for different forward detector acceptances. In our further calculations we fix  $\mu = \mu_0 = (m_W + m_t)/2$ .

### 3.4 Distribution and Cross Section

In Fig.9, we show the LO (solid curves) and NLO (dotted curves) transverse momentum ( $p_T$ ) distribution of W [left panel] and K-factor [right panel] for the process  $pp \rightarrow p\gamma p \rightarrow pWt + Y$ . (a), (b) and (c) for the experimental detector acceptances  $\xi_1$ ,  $\xi_2$  and  $\xi_3$ ,

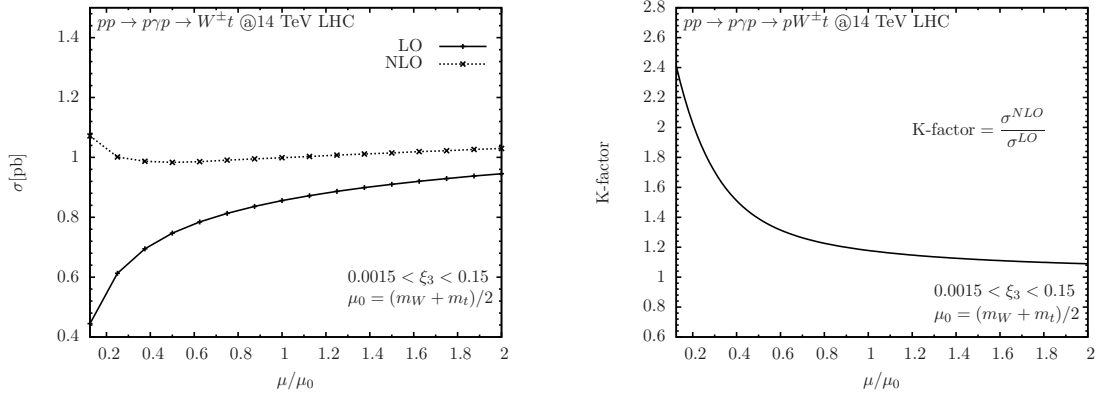
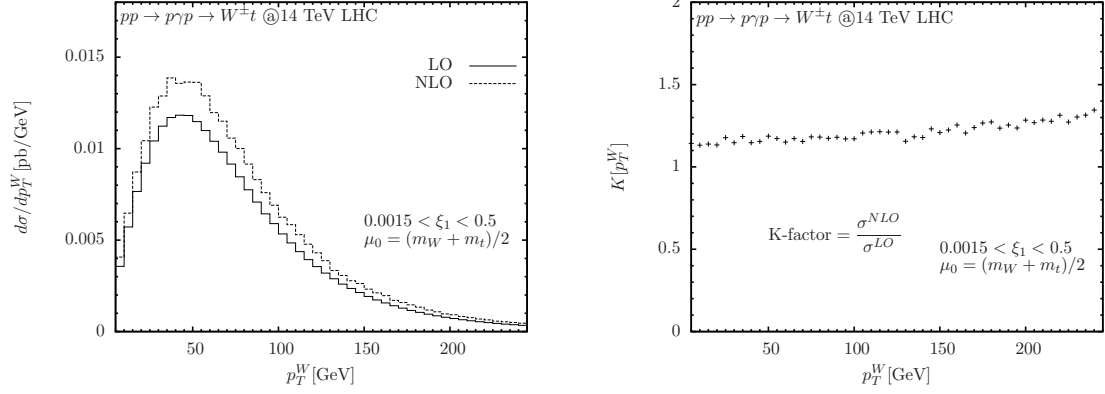


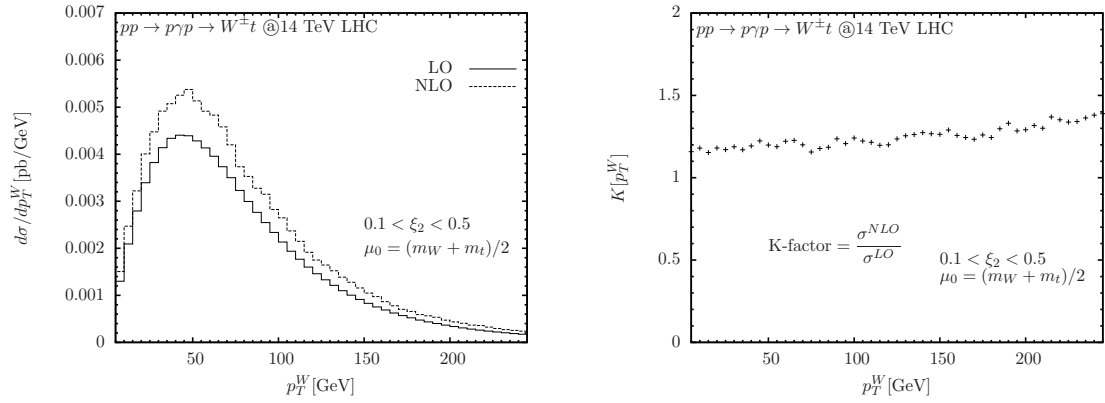
Figure 8: The scale- $\mu$  dependence of the LO and QCD NLO corrected cross sections [left panel] and K-factor [right panel] for  $pp \rightarrow p\gamma p \rightarrow pWt + Y$  at the  $\sqrt{s} = 14$  TeV LHC with  $\mu_0 = (m_W + m_t)/2$ ,  $\delta_s = 10^{-4}$  and  $\delta_c = \delta_s/100$ . The experimental acceptance here is chosen to be  $0.0015 < \xi_3 < 0.15$  for AFP-ATLAS forward detectors.

K-factor for $pp \rightarrow p\gamma p \rightarrow pWt + Y$				
$\xi \backslash \mu$	$\mu_0/8$	$\mu_0/2$	$\mu_0$	$2\mu_0$
$\xi_1$	2.4557	1.3415	1.1808	1.0947
$\xi_2$	2.5761	1.3997	1.2139	1.1069
$\xi_3$	2.4101	1.3166	1.1673	1.0892

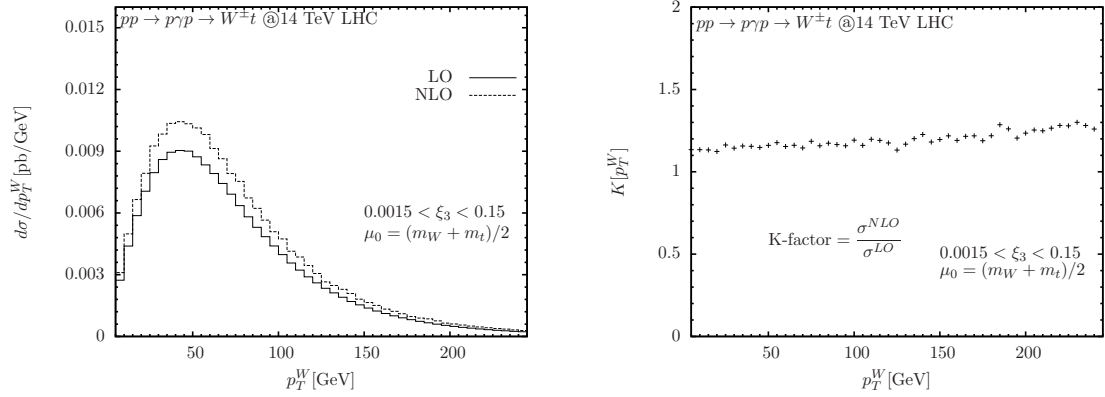
Table 3: The K-factor for typical value of  $\mu$  for different forward detector acceptances  $0.0015 < \xi_1 < 0.5$ ,  $0.1 < \xi_2 < 0.5$  and  $0.0015 < \xi_3 < 0.15$  with  $\mu_0 = (m_W + m_t)/2$ .



(a)  $0.0015 < \xi_1 < 0.5$



(b)  $0.1 < \xi_2 < 0.5$



(c)  $0.0015 < \xi_3 < 0.15$

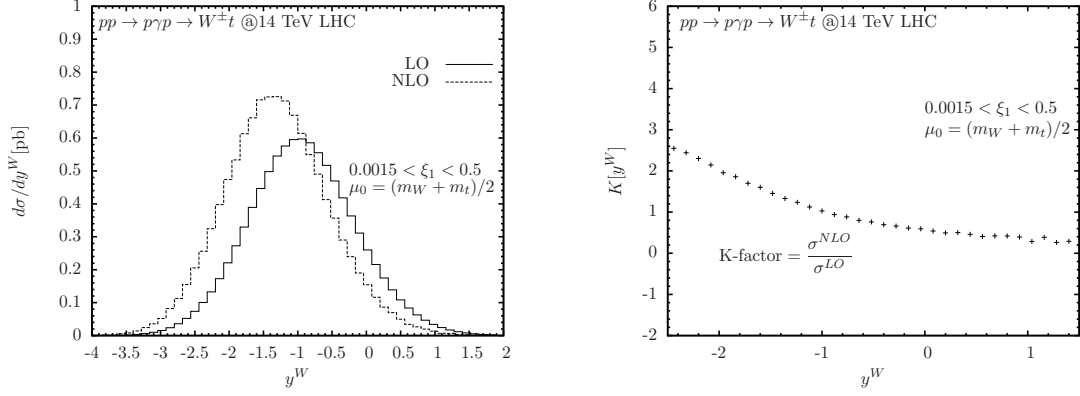
Figure 9: The LO (solid curves) and NLO (dotted curves) transverse momentum ( $p_T$ ) distribution of W [left panel] and K-factor [right panel] for the process  $pp \rightarrow p\gamma p \rightarrow pWt + Y$  at 14 TeV LHC with  $\mu = \mu_0 = (m_W + m_t)/2$ ,  $\delta_s = 10^{-4}$  and  $\delta_c = \delta_s/100$ . The experimental detector acceptances are  $0.0015 < \xi_1 < 0.5$ (a),  $0.1 < \xi_2 < 0.5$ (b),  $0.0015 < \xi_3 < 0.15$ (c).



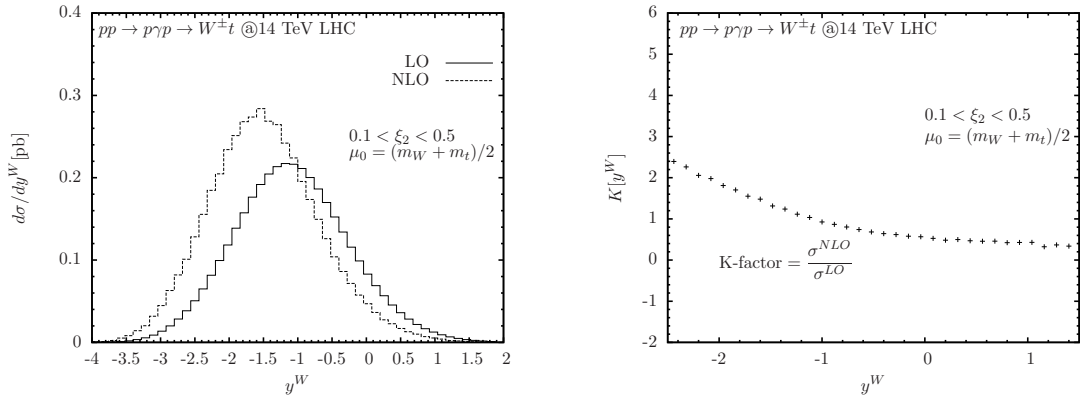
respectively. Of course the distributions depend on the detector acceptances, i.e., in the most efficient case  $0.0015 < \xi_1 < 0.5$ . However, their line behaviors are the same for different detector acceptances. For the distributions of  $p_T^{\text{top}}$ , their behaviors are very similar to those of  $p_T^W$  thus not shown. The results show that QCD NLO contribution can enhance the LO distribution in the whole  $p_T$  range. Typical K-factor is in the range of [1.1-1.4].

Rapidity distributions for the W boson and top quark have been presented in Fig.10 and Fig.11. As can be seen the NLO corrections can shift the LO rapidity but in different ways for both W boson and top quark. For the W boson the distribution  $y^W$ , QCD NLO corrections shift the LO peak range into different  $y$  and enhance them. For the top quark rapidity distributions there is not much enhancement can be found, instead, the rapidity values where they peaked shifts. Same behaviors but different values can be found for the other choices of  $\xi_2$  and  $\xi_3$  as can be see in Fig.10(a-c) and Fig.11(a-c), respectively. Their corresponding K-factors are present in the right panels. The reduction can be found for the K-factor when  $y^W$  increase from -4 to -1. With  $y^W < -0.8$  NLO correction enhance the LO predictions while reverse in the range  $y^W \geq -0.8$ . This behavior is the same for all three value of forward detector acceptances  $\xi_1$ ,  $\xi_2$  and  $\xi_3$ . For  $y^{\text{top}}$ , this value is around 0.2. That is to say, for  $y^{\text{top}} < 0.2$  NLO correction enhance the LO predictions while reverse in the range  $y^{\text{top}} \geq 0.2$ .

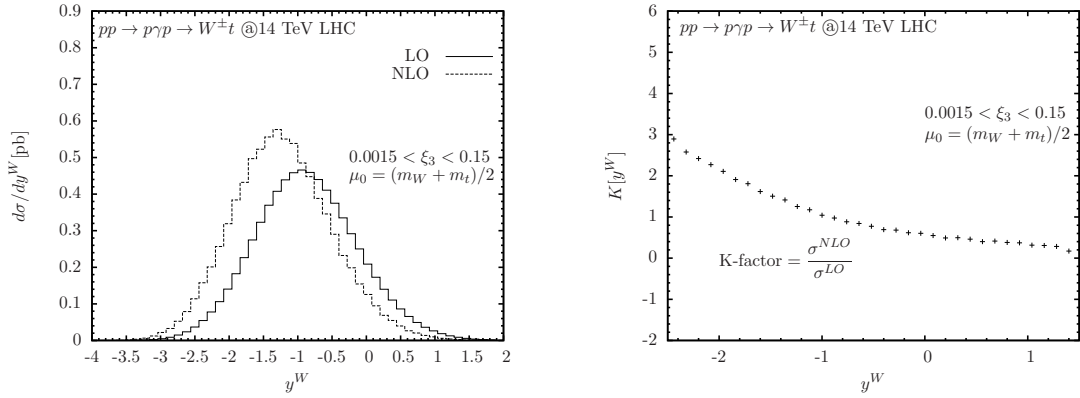
In Fig.12 we fix  $\xi_{\text{min}} = 0.0015$  and take  $\xi_{\text{max}}$  as a running parameter from 0.15 to 1. The LO and NLO cross sections as well as the the K-factor defined as  $\sigma^{\text{NLO}}/\sigma^{\text{LO}}$  are presented as functions of different values of  $\xi_{\text{max}}$ . The dotted, dashed and solid lines correspond to the LO, NLO predictions and K-factor, respectively. We can find that in the range  $0.0015 < \xi_{\text{max}} < 0.5$ , both LO and NLO predictions rely on the detector acceptances while in the region  $\xi_{\text{max}} > 0.5$ , little contributions will shift the LO and NLO cross sections. No matter how the detector acceptances changes, the ratio of  $\sigma^{\text{NLO}}$  to  $\sigma^{\text{LO}}$  does not change much where a typical value of K-factor equal 1.1808 in the massless assumption, leading the QCD NLO corrections up to 18.08% related to the LO predictions with our chosen parameters.



(a)  $0.0015 < \xi_1 < 0.5$

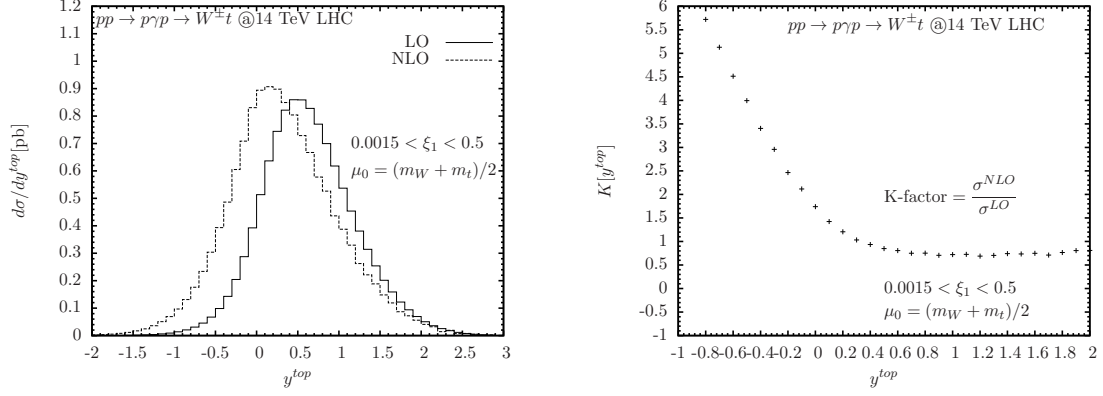


(b)  $0.1 < \xi_2 < 0.5$

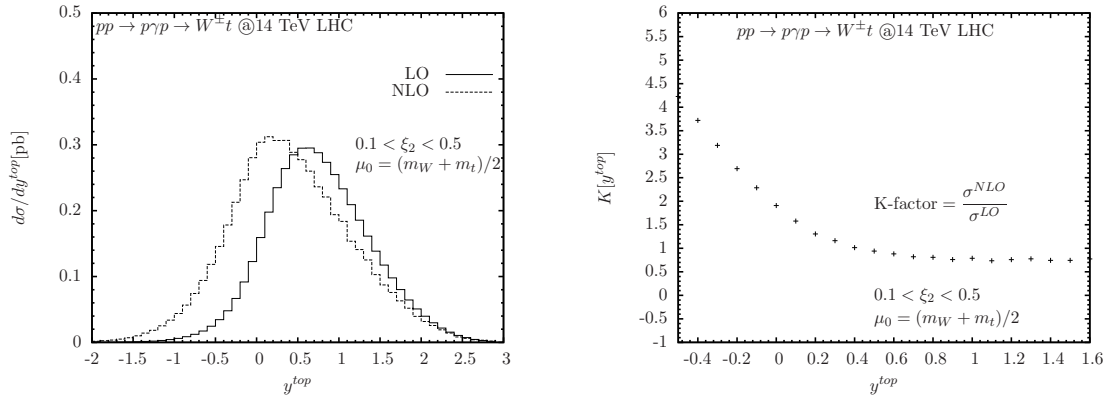


(c)  $0.0015 < \xi_3 < 0.15$

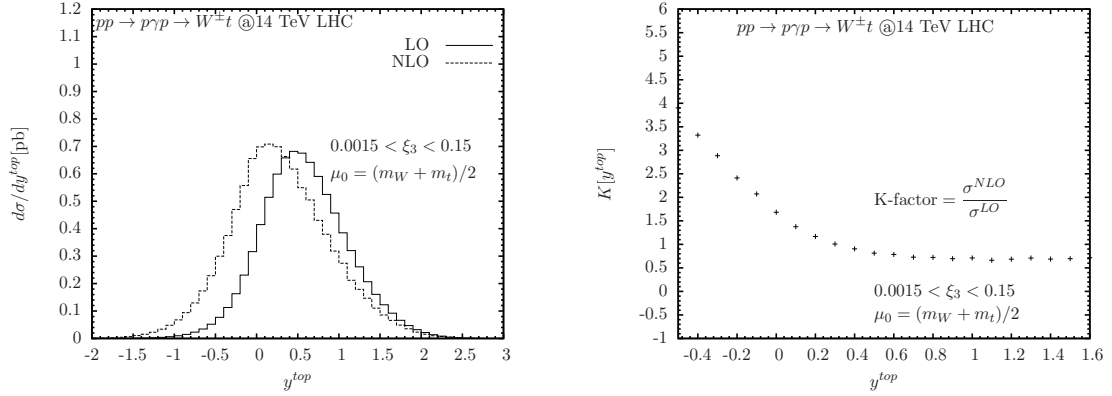
Figure 10: The LO (solid curves) and NLO (dotted curves) Rapidity ( $y$ ) distribution of  $W$  [left panel] and K-factor [right panel] for the process  $pp \rightarrow p\gamma p \rightarrow pWt + Y$  at 14 TeV LHC with  $\mu = \mu_0 = (m_W + m_t)/2$ ,  $\delta_s = 10^{-4}$  and  $\delta_c = \delta_s/100$ . The experimental detector acceptances are  $0.0015 < \xi_1 < 0.5$ (a),  $0.1 < \xi_2 < 0.5$ (b),  $0.0015 < \xi_3 < 0.15$ (c).



(a)  $0.0015 < \xi_1 < 0.5$



(b)  $0.1 < \xi_2 < 0.5$



(c)  $0.0015 < \xi_3 < 0.15$

Figure 11: The LO (solid curves) and NLO (dotted curves) Rapidity ( $y$ ) distribution of top [left panel] and K-factor [right panel] for the process  $pp \rightarrow p\gamma p \rightarrow pWt + Y$  at 14 TeV LHC with  $\mu = \mu_0 = (m_W + m_t)/2$ ,  $\delta_s = 10^{-4}$  and  $\delta_c = \delta_s/100$ . The experimental detector acceptances are  $0.0015 < \xi_1 < 0.5$ (a),  $0.1 < \xi_2 < 0.5$ (b),  $0.0015 < \xi_3 < 0.15$ (c).

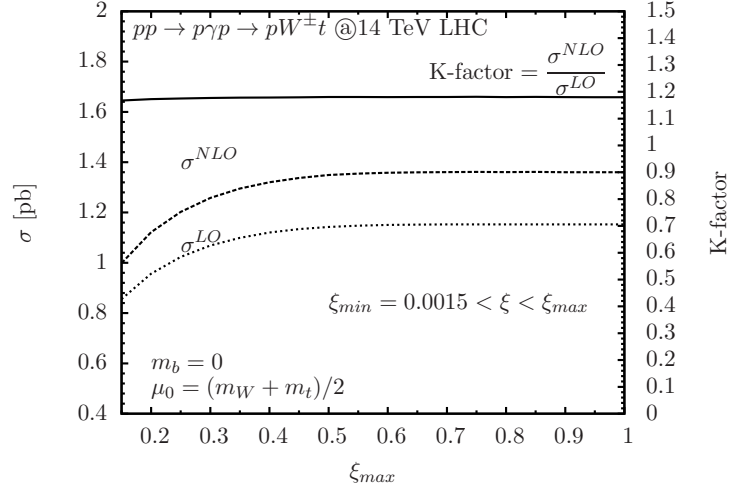


Figure 12: Cross sections for LO and NLO predictions for  $pp \rightarrow p\gamma p \rightarrow pWt + Y$  as well as the K-factor as functions of different values of  $\xi_{\max}$  at 14 TeV LHC. Here we fix  $\xi_{\min} = 0.0015$  and take  $\xi_{\max}$  as a running parameter from 0.15 to 1. The dotted, dashed and the solid line correspond to the LO, NLO predictions and K-factor, respectively.  $\mu = \mu_0 = (m_W + m_t)/2$ ,  $\delta_s = 10^{-4}$  and  $\delta_c = \delta_s/100$ .

## 4 Summary

In this work, we present the precise production of Single Top and W boson associated photoproduction up to NLO QCD level through the main reaction  $pp \rightarrow p\gamma p \rightarrow pW^{\pm}t + Y$  at the future 14 TeV Large Hadron Collider (LHC) for the first time, assuming a typical LHC multipurpose forward detector. We use the Five-Flavor-Number Schemes (5FNS) through the whole calculation while treat the initial state b quark as massless. This is the most important two body final state single top production channel at the  $\gamma p$  collision. By detecting this process we can certainly in analyses aiming at top quark electrical charge, top quark mass prediction, and the CKM matrix element  $|V_{tb}|$  and give complementary information for normal pp collisions. In this paper, we have employed equivalent photon approximation (EPA) for the incoming photon beams and performed detailed analysis for various forward detector acceptances ( $\xi$ ). We analyse their impacts on both the total cross section, renormalization/factorization scale  $\mu$  dependence and some key distributions. Our results show that: QCD NLO corrections can reduce the factorization and renormalization scale uncertainty correspond to their LO predictions. They can enhance the transverse momentum ( $p_T^{W^{\pm}, \text{top}}$ ) distributions and shift the LO predictions in different ways for  $y^{W^{\pm}}$  and  $y^{\text{top}}$ , leading some interesting behaviors and the crucial importance of considering the QCD NLO corrections. The typical QCD K-factor value in massless b quark scheme are 1.1808 for CMS-TOTEM forward detectors with  $0.0015 < \xi_1 < 0.5$ , 1.2139 for CMS-TOTEM forward detectors with  $0.1 < \xi_2 < 0.5$  and 1.1673 for AFP-ATLAS forward detectors with  $0.0015 < \xi_3 < 0.15$ , respectively, with our chosen parameters.

**Acknowledgments:** Sun Hao thanks Dr. Inanc Sahin for his kindness to provide invaluable comments, thanks Dr. RenYou Zhang for his strong support and thanks Dr. ChongXing Yue, Lei Guo, ShaoMing Wang for useful discussions. Project supported by the National Natural Science Foundation of China (Grant No. 11205070, 11105083, 11035003, 11375104, 11105036), by Shandong Province Natural Science Foun-

dation (Grant No. ZR2012AQ017), and by the Fundamental Research Funds for the Central Universities (No. DUT13RC(3)30).

## References

- [1] ATLAS Collaboration, *Combination of Higgs Boson Searches with up to  $4.9 \text{ fb}^{-1}$  of  $pp$  Collisions Data Taken at a center-of-mass energy of 7 TeV with the ATLAS Experiment at the LHC*, ATLAS-CONF-2011-163.
- [2] CMS Collaboration, *Combination of SM Higgs Searches*, CMS PAS HIG-11-032.
- [3] A. Abulencia, et al., (CDF Collaboration), *Observation of Exclusive Electron-Positron Production in Hadron-Hadron Collisions*, Phys. Rev. Lett. 98 (2007) 112001, [arXiv:hep-ex/0611040].
- [4] T. Aaltonen, et al., (CDF Collaboration), *Search for Exclusive Z-Boson Production and Observation of High-Mass  $p\bar{p} \rightarrow p\gamma\gamma\bar{p} \rightarrow p\ell^+\ell^-\bar{p}$  Events in  $p\bar{p}$  Collisions at  $\sqrt{s} = 1.96 \text{ TeV}$* , Phys. Rev. Lett. 102 (2009) 222002, [arXiv:0902.2816].
- [5] T. Aaltonen, et al., (CDF Collaboration), *Search for Exclusive  $\gamma\gamma$  Production in Hadron-Hadron Collisions*, Phys. Rev. Lett. 99 (2007) 242002, [arXiv:0707.2374]; *Observation of Exclusive  $\gamma\gamma$  Production in  $p\bar{p}$  Collisions at  $\sqrt{s} = 1.96 \text{ TeV}$* , Phys. Rev. Lett. 108 (2012) 081801, [arXiv:1112.0858].
- [6] T. Aaltonen, et al., (CDF Collaboration), *Observation of exclusive dijet production at the Fermilab Tevatron  $p\bar{p}$  collider*, Phys. Rev. D. 77 (2008) 052004, [arXiv:0712.0604].
- [7] T. Aaltonen, et al., (CDF Collaboration), *Observation of Exclusive Charmonium Production and  $\gamma\gamma \rightarrow \mu^+\mu^-$  in  $p\bar{p}$  Collisions at  $\sqrt{s} = 1.96 \text{ TeV}$* , Phys. Rev. Lett. 102 (2009) 242001, [arXiv:0902.1271].

- [8] M. Tasevsky, *Diffraction physics program in ATLAS experiment*, Nucl. Phys. Proc. Suppl. 179-180 (2008) 187-195, ATL-PHYS-CONF-2008-019, ATL-COM-PHYS-2008-087; *Measuring Central Exclusive Processes at LHC*, [arXiv:0910.5205].
- [9] C. Royon, (RP220 Collaboration), *Project to install roman pot detectors at 220 m in ATLAS*, [arXiv:0706.1796]; M.G. Albrow, et al., *FP420: An R&D proposal to investigate the feasibility of installing proton tagging detectors in the 420-m region at LHC*, CERN-LHCC-2005-025; B.E. Cox, (FP420 R and D Collaboration), *The FP420 R&D Project at the LHC*, [arXiv:hep-ph/0609209].
- [10] Marek Tasevsky, *Review of Central Exclusive Production of the Higgs Boson Beyond the Standard Model*, to appear as review article in Int J Mod Phys A, [arXiv:1407.8332].
- [11] C. Royon, *The ATLAS Forward Physics Project*, [arXiv:1302.0623].
- [12] R. Staszewski, (ATLAS Collaboration), *The AFP Project*, Acta Physica Polonica B vol. 42 (2011) 1615, [arXiv:1104.1858].
- [13] J. de Favereau de Jeneret, V. Lemaître, Y. Liu, S. Ovyn, T. Pierzchala, K. Piotrzkowski, X. Rouby, N. Schul, M. Vander Donckt, *High energy photon interactions at the LHC*, [arXiv:0908.2020].
- [14] Tim M. P. Tait,  *$tW^-$  mode of single top quark production*, Phys. Rev. D 61 (1999) 034001, [arXiv:hep-ph/9909352].
- [15] J. Alwall, R. Frederix, J.-M. Gerard, A. Giammanco, M. Herquet, S. Kalinin, E. Kou, V. Lemaître, F. Maltoni, *Is  $V_{tb}=1$  ?*, Eur. Phys. J. C 49 (2007) 791-801, [arXiv:hep-ph/0607115].
- [16] J. A. Aguilar-Saavedra, A. Onofre, *Using single top rapidity to measure  $V_{td}$ ,  $V_{ts}$ ,  $V_{tb}$  at hadron colliders*, Phys. Rev. D 83 (2011) 073003, [arXiv:1002.4718].

- [17] CMS collaboration, *CMS Physics Technical Design Report, Volume II: Physics Performance*, J. Phys. G: Nucl. Part. Phys. 34 (2007) 995-1579.
- [18] A. S. Belyaev, E. E. Boos, L. V. Dudko, *Single Top Quark at Future Hadron Colliders. Complete Signal and Background Study*, Phys. Rev. D 59 (1999) 075001, [arXiv:hep-ph/9806332].
- [19] S. Ovin, J. de Favereau de Jeneret, *High energy single top photoproduction at the LHC*, Nuovo Cim. B 123 (2008) 1126-1133, [arXiv:0806.4841].
- [20] J. de Favereau de Jeneret, S. Ovin, *Single top quark photoproduction at the LHC*, Nucl. Phys. Proc. Suppl. 179-180 (2008) 277-284, [arXiv:0806.4886].
- [21] The CMS Collaboration, J. Phys. G, 34 (2007) 1227-1237.
- [22] S. Atag, O. Cakir, B. Dilec, *Anomalous Wtb Coupling in ep Collision*, Phys. Lett. B 522 (2001) 76-82, [arXiv:hep-ph/0107179].
- [23] Sukanta Dutta, Ashok Goyal, Mukesh Kumar, Bruce Mellado, *Measuring anomalous Wtb couplings at  $e^-p$  collider*, [arXiv:1307.1688].
- [24] V. M. Abazov, et al., (D0 Collaboration), *Observation of Single Top-Quark Production* Phys. Rev. Lett. 103 (2009) 092001, [arXiv:0903.0850]; V. M. Abazov, et al., (D0 Collaboration), *Measurement of the  $t$ -channel single top quark production cross section*, Phys. Lett. B 682 (2010) 363, [arXiv:0907.4259]; T. Aaltonen, et al., (CDF Collaboration), *First Observation of Electroweak Single Top Quark Production*, Phys. Rev. Lett. 103 (2009) 092002, [arXiv:0903.0885].
- [25] Douglas O. Carlson, C.P. Yuan, *Studying the top quark via the  $W$ -gluon fusion process*, Phys. Lett. B 306 (1993) 386; Gregory Mahlon, Stephen Parke, *Improved Spin Basis for Angular Correlation Studies in Single Top Quark Production at the Tevatron* Phys. Rev. D 55 (1997) 7249-7254, [arXiv:hep-ph/9611367]; A. P. Heinson, A. S. Belyaev, E. E. Boos, *Single top quarks at the Fermilab Tevatron*, Phys. Rev. D 56



- (1997) 3114-3128, [arXiv:hep-ph/9612424]; Gregory Mahlon, Stephen Parke, *Single Top Quark Production at the LHC: Understanding Spin*, Phys. Lett. B 476 (2000) 323-330, [arXiv:hep-ph/9912458]; Zack Sullivan, *Angular correlations in single-top-quark and  $Wjj$  production at next-to-leading order* Phys. Rev. D 72 (2005) 094034, [arXiv:hep-ph/0510224].
- [26] C. E. Gerber et al., (The TeV4LHC-Top and Electroweak Working Group), *Tevatron-for-LHC Report: Top and Electroweak Physics*, Report No. FERMILAB-CONF-07-052 (2007), [arXiv:0705.3251] and references therein.
- [27] B. Sahin, A. A. Billur, *Anomalous  $Wtb$  couplings in  $\gamma p$  collision at the LHC*, Phys. Rev. D 86 (2012) 074026, [arXiv:1210.3235].
- [28] O. Kepka, C. Royon, *Anomalous  $WW\gamma$  coupling in photon-induced processes using forward detectors at the CERN LHC*, Phys. Rev. D 78 (2008) 073005, [arXiv:0808.0322].
- [29] I. Sahin, A. A. Billur, *Anomalous  $WW\gamma$  couplings in  $\gamma p$  collision at the LHC*, Phys. Rev. D 83 (2011) 035011, [arXiv:1101.4998].
- [30] C. Royon, E. Chapon, O. Kepka, *Anomalous trilinear and quartic  $WW\gamma$ ,  $WW\gamma\gamma$ ,  $ZZ\gamma$  and  $ZZ\gamma\gamma$  couplings in photon induced processes at the LHC*, PoS EPS-HEP2009 (2009) 380, [arXiv:0909.5237].
- [31] I. Sahin, B. Sahin, *Anomalous quartic  $ZZ\gamma\gamma$  couplings in  $\gamma p$  collision at the LHC*, Phys. Rev. D 86 (2012) 115001, [arXiv:1211.3100].
- [32] A. Senol,  *$ZZ\gamma$  and  $Z\gamma\gamma$  anomalous couplings in  $\gamma p$  collision at the LHC*, Phys. Rev. D 87 (2013) 073003, [arXiv:1301.6914].
- [33] A. Senol, *Anomalous quartic  $WW\gamma\gamma$  and  $ZZ\gamma\gamma$  couplings in  $\gamma p$  collision at the LHC*, [arXiv:1311.1370].

- [34] M.Köksal, S. C. Inan, *Anomalous  $tq\gamma$  couplings in  $\gamma p$  collision at the LHC*, Advances in High Energy Physics, Volume 2014, Article ID 935840, [arXiv:1305.7096].
- [35] Hao Sun, *Probe Anomalous  $tq\gamma$  couplings through Single Top Photoproduction at the LHC*, Nucl. Phys. B 886 (2014) 691-711, [arXiv:1402.1817].
- [36] Sarah Heim, Qing-Hong Cao, Reinhard Schwienhorst, C.-P. Yuan, *Next-to-leading order QCD corrections to s-channel single top quark production and decay at the LHC*, Phys. Rev. D 81 (2010) 034005, [arXiv:0911.0620].
- [37] Walter T. Giele, Stephane Keller, Eric Laenen, *QCD Corrections to W Boson plus Heavy Quark Production at the Tevatron*, Phys. Lett. B 372 (1996) 141-149, [arXiv:hep-ph/9511449].
- [38] Shou-hua Zhu, *Next-to-leading order QCD corrections to  $b\bar{g} \rightarrow tW^-$  at the CERN Large Hadron Collider*, Phys. Lett. B 524 (2002) 283-88, Erratum-ibid. B 537 (2002) 351, [arXiv:hep-ph/0109269].
- [39] Qing-Hong Cao, *Demonstration of One Cutoff Phase Space Slicing Method: Next-to-Leading Order QCD Corrections to the  $tW$  Associated Production in Hadron Collision*, [arXiv:0801.1539].
- [40] M. Beccaria, C.M. Carloni Calame, G. Macorini, G. Montagna, F. Piccinini, F.M. Renard, C. Verzegnassi, *A complete one-loop description of associated  $tW$  production at LHC and an estimate of possible genuine supersymmetric effects*, Eur. Phys. J. C 53 (2008) 257-265, [arXiv:0705.3101].
- [41] S. Frixione, E. Laenen, P. Motylinski, B. Webber, C. D. White, *Single-top hadroproduction in association with a W boson*, JHEP 0807 (2008) 029, [arXiv:0805.3067].
- [42] John Campbell, Francesco Tramontano, *Next-to-leading order corrections to  $Wt$  production and decay*, Nucl. Phys. B 726 (2005) 109-130, [arXiv:hep-ph/0506289].

- [43] F. Cascioli, S. Kallweit, P. Maierhöfer, S. Pozzorini *A unified NLO description of top-pair and associated  $Wt$  production*, Eur. Phys. J. C 74 (2014) 2783, [arXiv:1312.0546].
- [44] V. M. Budnev, I. F. Ginzburg, G. V. Meledin, V. G. Serbo, *The two-photon particle production mechanism. Physical problems. Applications. Equivalent photon approximation*, Phys. Rep. 15 (1975) 181; G. Baur, K. Hencken, D. Trautmann, S. Sadowsky and Y. Kharlov, *Coherent  $\gamma\gamma$  and  $\gamma A$  interactions in very peripheral collisions at relativistic ion colliders*, Phys. Rep. 364 (2002) 359, [arXiv:hep-ph/0112211]; K. Piotrkowski, *Tagging two-photon production at the CERN Large Hadron Collider*, Phys. Rev. D 63 (2001) 071502, [hep-ex/0009065].
- [45] S. Oryn, *Associated  $W$  and Higgs boson photoproduction and other electroweak photon induced processes at the LHC*, Nucl. Phys. Proc. Suppl. 179-180 (2008) 269-276, [arXiv:0806.1157].
- [46] N. Schul, K. Piotrkowski, *Detection of two-photon exclusive production of supersymmetric pairs at the LHC*, Nucl. Phys. Proc. Suppl. 179-180 (2008) 289-297, [arXiv:0806.1097]; K. Piotrkowski, N. Schul, *Two-photon exclusive production of supersymmetric pairs at the LHC*, AIP Conf.Proc. 1200 (2010) 434-437, [arXiv:0910.0202].
- [47] S. Heinemeyer, V. A. Khoze, M. G. Ryskin, W. J. Stirling, M. Tasevsky, G. Weiglein, *Studying the MSSM Higgs sector by forward proton tagging at the LHC*, Eur. Phys. J. C 53 (2008) 231-256, [arXiv:0708.3052]; S. Heinemeyer, V. A. Khoze, M. Tasevsky, G. Weiglein, *Exclusive Production of the MSSM Higgs Bosons at the LHC*, [arXiv:1206.0183]; S. Heinemeyer, V.A. Khoze, M.G. Ryskin, M. Tasevsky, G. Weiglein, *BSM Higgs Physics in the Exclusive Forward Proton Mode at the LHC*, Eur. Phys. J. C 71 (2011) 1649, [arXiv:1012.5007]; Marek Tasevsky, *Exclusive MSSM Higgs production at the LHC after Run I*, Eur. Phys. J. C 73 (2013) 2672, [arXiv:1309.7772].
- [48] S. Atag, S.C. Inan, I. Sahin, *Extra dimensions in photon-induced two lepton final states at the CERN-LHC*, Phys. Rev. D 80 (2009) 075009, [arXiv:0904.2687].

- [49] S. Atag, S.C. Inan, I. Sahin, *Extra dimensions in  $\gamma\gamma \rightarrow \gamma\gamma$  process at the CERN-LHC*, JHEP 09 (2010) 042, [arXiv:1005.4792].
- [50] Hao Sun, *Large Extra Dimension effects through Light-by-Light Scattering at the CERN LHC*, Eur. Phys. J. C 74 (2014) 2977, [arXiv:1406.3897].
- [51] I. Sahin, A.A. Billur, S.C. Inan, B. Sahin, M. Koksall, P. Tektas, E. Alici, R. Yildirim, *Probe of extra dimensions in  $\gamma q \rightarrow \gamma q$  at the LHC*, Phys. Rev. D 88 (2013) 095016, [arXiv:1304.5737].
- [52] I. Sahin, S. C. Inan, *Probe of unparticles at the LHC in exclusive two lepton and two photon production via photon-photon fusion*, JHEP 0909 (2009) 069, [arXiv:0907.3290].
- [53] Hao Sun, Chong-Xing Yue, *Precise photoproduction of the charged top-pions at the LHC with forward detector acceptances*, Eur. Phys. J. C 74 (2014) 2823, [arXiv:1401.0250].
- [54] T. Pierzchała, K. Piotrkowski, *Sensitivity to anomalous quartic gauge couplings in photon-photon interactions at the LHC*, Nucl.Phys.Proc.Suppl. 179-180 (2008) 257-264, [arXiv:0807.1121].
- [55] E. Chapon, C. Royon, O. Kepka, *Anomalous quartic  $WW\gamma\gamma$ ,  $ZZ\gamma\gamma$ , and trilinear  $WW\gamma$  couplings in two-photon processes at high luminosity at the LHC*, Phys. Rev. D 81 (2010) 074003, [arXiv:0912.5161].
- [56] Rick S. Gupta, *Probing quartic neutral gauge boson couplings using diffractive photon fusion at the LHC*, Phys. Rev. D 85 (2012) 014006, [arXiv:1111.3354].
- [57] S. Fichet, G. von Gersdorff, O. Kepka, B. Lenzi, C. Royon, M. Saimpert, *Probing new physics in diphoton production with proton tagging at the Large Hadron Collider*, [arXiv:1312.5153].

- [58] I. Sahin, M. Koksak, *Search for electromagnetic properties of the neutrinos at the LHC*, JHEP 1103 (2011) 100, [arXiv:1010.3434].
- [59] S. Atag, A.A. Billur, *Possibility of Determining  $\tau$  Lepton Electromagnetic Moments in  $\gamma\gamma \rightarrow \tau^+\tau^-$  Process at the CERN-LHC*, JHEP 1011 (2010) 060, [arXiv:1005.2841].
- [60] I. Sahin, *Electromagnetic properties of the neutrinos in gamma-proton collision at the LHC*, Phys. Rev. D 85 (2012) 033002, [arXiv:1201.4364].
- [61] Hao Sun, *Dark Matter Searches in Jet plus Missing Energy in  $\gamma p$  collision at CERN LHC*, Phys. Rev. D 90 (2014) 035018, D, [arXiv:1407.5356].
- [62] M. Chaichian, P. Hoyer, K. Huitu, V.A. Khoze, A.D. Pilkington, *Searching for the triplet Higgs sector via central exclusive production at the LHC*, JHEP 0905 (2009) 011, [arXiv:0901.3746].
- [63] S. Dawson, C.B. Jackson, L. Reina, D. Wackerroth, *Higgs boson production with one bottom quark jet at hadron colliders*, Phys. Rev. Lett. 94 (2005) 031802, [arXiv:hep-ph/0408077].
- [64] Stefan Dittmaier, Michael Krämer, Michael Spira, Manuel Walser, *Charged-Higgs-boson production at the LHC: NLO supersymmetric QCD corrections*, Phys. Rev. D 83 (2011) 055005, [arXiv:0906.2648].
- [65] John M. Campbell, Rikkert Frederix, Fabio Maltoni, Francesco Tramontano, *Next-to-leading-order predictions for  $t$ -channel single-top production at hadron colliders*, Phys. Rev. Lett. 102 (2009) 182003, [arXiv:0903.0005].
- [66] F. Caola, J.M. Campbell, F. Febres Cordero, L. Reina, D. Wackerroth, *NLO QCD predictions for  $W + 1$  jet and  $W + 2$  jet production with at least one  $b$  jet at the 7 TeV LHC*, Phys. Rev. D 86 (2012) 034021, [arXiv:1107.3714].

- [67] Robert Harlander, Michael Krämer, Markus Schumacher, *Bottom-quark associated Higgs-boson production: reconciling the four- and five-flavour scheme approach*, CERN-PH-TH/2011-134, [arXiv:1112.3478].
- [68] Malgorzata Worek, *NLO mass effects in  $b\bar{b}b\bar{b}$  production at the LHC*, PoS RADCOR 2013 (2013) 038, [arXiv:1311.2396].
- [69] H. B. Hartanto, L. Reina, *Hard-photon production with  $b$  jets at hadron colliders*, Phys. Rev. D 89 (2014) 074001, [arXiv:1312.2384].
- [70] Fabio Maltoni, Giovanni Ridolfi, Maria Ubiali,  *$b$ -Initiated processes at the LHC: a reappraisal*, JHEP 1207 (2012) 022, Erratum-ibid. 1304 (2013) 095, [arXiv:1203.6393].
- [71] John M. Campbell, Rikkert Frederix, Fabio Maltoni, Francesco Tramontano, *Next-to-leading-order predictions for  $t$ -channel single-top production at hadron colliders*, Phys. Rev. Lett. 102 (2009) 182003, [arXiv:0903.0005]; J. Campbell, R. Keith Ellis, F. Febres Cordero, F. Maltoni, L. Reina, D. Wackerroth, S. Willenbrock, *Associated Production of a  $W$  Boson and One  $b$  Jet*, Phys. Rev. D 79 (2009) 034023, [arXiv:0809.3003]; F. Caola, J.M. Campbell, F. Febres Cordero, L. Reina, D. Wackerroth, *NLO QCD predictions for  $W + 1$  jet and  $W + 2$  jet production with at least one  $b$  jet at the 7 TeV LHC*, Phys. Rev. D 86 (2012) 034021, [arXiv:1107.3714].
- [72] F. Febres Cordero, L. Reina, D. Wackerroth, *NLO QCD corrections to  $Z b$  anti- $b$  production with massive bottom quarks at the Fermilab Tevatron*, Phys. Rev. D 78 (2008) 074014, [arXiv:0806.0808]; F. Febres Cordero, L. Reina, D. Wackerroth, *NLO QCD corrections to  $W$  boson production with a massive  $b$ -quark jet pair at the Fermilab Tevatron  $p$ - $\bar{p}$  collider* Phys. Rev. D 74 (2006) 034007, [arXiv:hep-ph/0606102];  *$W$ - and  $Z$ -boson production with a massive bottom-quark pair at the Large Hadron Collider*, Phys. Rev. D 80 (2009) 034015, [arXiv:0906.1923]; *Associated production of a  $W$  or  $Z$  boson with bottom quarks at the Tevatron and the LHC*, PoS(RADCOR2009) 055, [arXiv:1001.3362].

- [73] B. W. Harris, J. F. Owens, *The two cutoff phase space slicing method*, Phys. Rev. D 65 (2002) 094032, [arXiv:hep-ph/0102128].
- [74] T. Hahn, *Generating Feynman diagrams and amplitudes with FeynArts 3*, Comput. Phys. Commun. 140 (2001) 418-431, [arXiv:hep-ph/0012260].
- [75] T. Hahn, *Automatic Loop Calculations with FeynArts, FormCalc, and LoopTools*, Nucl. Phys. Proc. Suppl. 89 (2000) 231-236, [arXiv:hep-ph/0005029]. S. Agrawal, T. Hahn, E. Mirabella, *FormCalc 7*, J. Phys. Conf. Ser. 368 (2012) 012054, [arXiv:1112.0124].
- [76] T. Hahn, M. Perez-Victoria, *Automatized one loop calculations in four-dimensions and D-dimensions*, Comput. Phys. Commun. 118 (1999) 153-165, [arXiv:hep-ph/9807565].
- [77] A. van Hameren, *OneLOop: for the evaluation of one-loop scalar functions*, Comput. Phys. Commun. 182 (2011) 2427-2438, [arXiv:1007.4716].
- [78] R. K. Ellis and G. Zanderighi, *Scalar one-loop integrals for QCD*, JHEP 0802 (2008) 002, [arXiv:0712.1851].
- [79] Tim M. P. Tait, *The  $tW^-$  Mode of Single Top Production*, Phys. Rev. D 61 (2000) 034001, [arXiv:hep-ph/9909352].
- [80] A. Belyaev, E. Boos, *Single top quark  $tW + X$  production at the LHC: a closer look*, Phys. Rev. D 63 (2001) 034012, [arXiv:hep-ph/0003260].
- [81] B. P. Kersevan, I. Hinchliffe, *A consistent prescription for the production involving massive quarks in hadron collisions*, JHEP 0609 (2006) 033, [arXiv:hep-ph/0603068].
- [82] T. Plehn, C. Weydert, *Charged Higgs production with a top in MC NLO*, PoS CHARGED 2010 (2010) 026, [arXiv:1012.3761]; T. Binoth, D. Goncalves-Netto, D. Lopez-Val, K. Mawatari, T. Plehn, I. Wigmore, *Automized Squark-Neutralino Production to Next-to-Leading Order*, Phys. Rev. D 84 (2011) 075005, [arXiv:1108.1250].

- [83] Zhang Ren-You, Yan Han, Ma Wen-Gan, Wang Shao-Ming, Guo Lei, Han Liang,  *$W_H/Z_H$  production associated with a  $T$ -odd (anti)quark at the LHC in NLO QCD*, Phys. Rev. D 85 (2012) 015017, [arXiv:1112.5225].
- [84] Dorival Goncalves-Netto, David Lopez-Val, Kentarou Mawatari, Tilman Plehn, Ioan Wigmore, *Sgluon Pair Production to Next-to-Leading Order*, Phys. Rev. D. 85 (2012) 114024, [arXiv:1203.6358].
- [85] Wolfgang Hollik, Jonas M. Lindert, Davide Pagani, *NLO corrections to squark-squark production and decay at the LHC*, JHEP 1303 (2013) 139, [arXiv:1207.1071].
- [86] Benjamin Fuks, Michael Klasen, David R. Lamprea, Marcel Rothering, *Gaugino production in proton-proton collisions at a center-of-mass energy of 8 TeV*, JHEP 1210 (2012) 081, [ arXiv:1207.2159].
- [87] L. Lewin, *Polylogarithms and associated functions*, North-Holland, Amsterdam, The Netherlands (1983).
- [88] W. Beenakker, H. Kuijf, and W. L. van Neerven, *QCD corrections to heavy-quark production in  $p\bar{p}$  collisions*, Phys. Rev. D 40 (1989) 54-82.
- [89] J. Beringer et al., (Particle Data Group), *Review of Particle Physics (RPP)*, Phys. Rev. D 86 (2012) 010001.
- [90] M.R. Whalley, D. Bourilkov, R. C. Group, *The Les Houches accord PDFs (LHAPDF) and LHAGLUE*, [arXiv:hep-ph/0508110].
- [91] J. Pumplin, D. R. Stump, J. Huston, H.L. Lai, P. M. Nadolsky, and W.K. Tung, *New generation of parton distributions with uncertainties from global QCD analysis*, JHEP 0207 (2002) 012, [arXiv:hep-ph/0201195]; D. Stump, J. Huston, J. Pumplin, W.-K. Tung, H.L. Lai, S. Kuhlmann, J.F. Owens, *Inclusive jet production, parton distributions, and the search for new physics*, JHEP 0310 (2003) 046.



- [92] S. Kawabata, *A new version of the multi-dimensional integration and event generation package BASES/SPRING*, Comp. Phys. Commun 88 (1995) 309-326; F. Yuasa, D. Perret-Gallix, S. Kawabata, T. Ishikawa, *Pvm-grace*, Nucl. Instrum. Meth. A389 (1997) 77-80.
- [93] Hameren A van, *Kaleu: a general-purpose parton-level phase space generator*, [arXiv:1003.4953].